

# 1 Optimal Ammonia Bunkering Infrastructure for Green Shipping Corridors: A Multi-Period Mixed-Integer Linear Programming Approach

---

## 1.1 Abstract

Ammonia is a leading zero-carbon marine fuel candidate, yet no quantitative framework exists for sizing the port-level bunkering infrastructure – shuttle vessels, pumps, and storage – required to deliver it from production facilities to ship fuel tanks. We formulate a mixed-integer linear programming (MILP) model that systematically evaluates all feasible shuttle-pump combinations and optimizes fleet deployment for each configuration over a 21-year planning horizon (2030–2050) for three ammonia supply chain configurations at Busan Port: port-based storage (Case 1), remote supply from Ulsan at 59 nm (Case 2), and remote supply from Yeosu at 86 nm (Case 3). Demand grows linearly from 50 to 500 ammonia-fueled vessels at 12 voyages per year. At a bunkering pump rate of 500 m<sup>3</sup>/h, the model identifies distinct optimal configurations: Case 1 selects a 1,000 m<sup>3</sup> shuttle at a 21-year net present cost (NPC) of \$447.53M and leveled cost of ammonia bunkering (LCOA) of \$1.90/ton, while Cases 2 and 3 require larger 5,000 m<sup>3</sup> shuttles at 2.0–2.4 times higher cost (\$906.80M and \$1,094.12M respectively). A parametric break-even distance analysis shows that port-based storage dominates remote supply at all distances within 10–200 nm when each configuration uses its own optimal shuttle size. Sensitivity analysis across four demand scenarios (250–1,000 end-vessels) demonstrates that optimal shuttle specifications are invariant, with LCOA varying only 3.7% for Case 1. These results provide port authorities with quantitative decision tools for ammonia bunkering infrastructure investment in green shipping corridors.

**Keywords:** ammonia bunkering; green shipping corridor; mixed-integer linear programming; fleet sizing; leveled cost; infrastructure optimization

---

## 1.2 1. Introduction

The International Maritime Organization (IMO) has adopted a revised GHG strategy targeting at least 30% emission reduction by 2030, 80% by 2040, and net-zero by or around 2050 relative to 2008 levels [5, 29]. Achieving these targets requires a transition from conventional marine fuels to zero-carbon alternatives. Among the candidates, ammonia (NH<sub>3</sub>) has emerged as a leading option due to its zero-carbon combustion, existing global production infrastructure (~180 million tons/year), and compatibility with established bulk liquid transport methods [1, 2]. Green ammonia production costs are projected to decline from \$720–\$1,400/ton (2022) to \$310–\$610/ton by 2050 [31], making it increasingly competitive as a marine fuel. As of December 2025, 144 ammonia-fueled vessels and 302 ammonia-ready vessels have been ordered, signaling that the demand side of the ammonia fuel transition is materializing. The supply side – specifically, the port-level infrastructure required to deliver ammonia from production facilities to vessel fuel tanks – remains unresolved.

Green shipping corridor initiatives aim to bridge this gap by establishing end-to-end infrastructure for

zero-emission vessel operations along specific trade routes. The Korea–United States green corridor agreement (formalized April 2025) targets ammonia-fueled container ship operations between Busan and Seattle-Tacoma by 2027, with the Korean government investing approximately \$10 billion in Busan mega-port infrastructure including alternative fuel bunkering facilities [6]. Similar corridors are planned between Korea and Australia. These initiatives specify the fuel (ammonia) and the endpoints (ports) but leave a fundamental operational question unanswered: what bunkering infrastructure – shuttle vessels, pumps, and storage facilities – is required, at what scale, and when should it be deployed?

### 1.2.1 1.1 Related Work

The technical viability of ammonia as a marine fuel has been established through multiple review papers and techno-economic assessments. Al-Enazi et al. [1] provided a comprehensive comparison of alternative marine fuels, identifying ammonia’s advantages (zero-carbon combustion, existing transport infrastructure at -33 C) and disadvantages (toxicity, lower energy density than LNG). Imhoff et al. [2] quantified ammonia engine performance through thermodynamic simulation, establishing specific fuel oil consumption (SFOC) values that feed into operational cost estimates. Kim et al. [3] evaluated the economics of ammonia-fueled propulsion for individual vessels, finding cost premiums of 1.5–2.5x over conventional fuels depending on ammonia price assumptions. Korberg et al. [4] synthesized techno-economic parameters, and Wang and Wright [10] compared bunkering infrastructure requirements across fuel types qualitatively. All five studies treat the bunkering supply chain as a fixed assumption – ammonia is available at a given price and location – without asking how the ammonia reaches the vessel, what infrastructure is required to deliver it, or how that infrastructure should be sized.

At the strategic level, the green corridor concept has gained institutional support through the Getting to Zero Coalition [6], which identified Busan as a candidate port for a Korea–Australia ammonia shipping corridor. Lloyd’s Register and UMAS [7] estimated fuel transition costs at a macro level, Xing et al. [5] mapped decarbonization pathways through 2050, and Verschuur et al. [37] quantified the socio-economic and environmental impacts of green corridor infrastructure investments. The Korean government’s 2023 National Action Plan (“Toward Green Shipping by 2050”) establishes policy targets, and the IMO’s 2023 revised GHG strategy [30] sets binding emission reduction milestones that create the demand trajectory underlying our model. However, these documents set targets (number of zero-emission vessels, percentage of green fuel) without providing decision-makers with quantitative tools to determine how many shuttle vessels to procure, what capacity those vessels should have, or when to expand the fleet.

The most directly relevant operational study is Yang and Lam [11], who developed a discrete event simulation (DES) model for ammonia bunkering supply chains at port. Their model evaluates how the number and capacity of ammonia bunker supply vessels, bunkering flow rate, and demand level affect operational and economic performance. Key findings include: flow rate has up to 51.3% impact on bunkering service time (when varied by +/-50%), and the number of bunker supply vessels is the most sensitive parameter for annual operational cost (up to 15.2% effect). Their DES model evaluates predefined configurations through simulation runs – it answers “what happens if we deploy N vessels of size S?” but does not identify the optimal N and S. Furthermore, their model uses static demand (a fixed number of vessels requiring bunkering), whereas operational planning requires modeling demand as a trajectory over time. They also analyze a single

supply chain configuration rather than comparing port-based storage versus remote supply alternatives.

A complementary body of work has emerged on ammonia bunkering safety. Fan et al. [18] developed the first Bayesian network-based quantitative risk assessment for ammonia ship-to-ship bunkering, finding that toxicity poses greater risk than flammability. Yang and Lam [19] extended this to multi-scale release analysis, and Kim et al. [20] integrated STPA with Bayesian networks for port-level ammonia bunkering risk. Qu et al. [35] proposed a comprehensive QRA framework for ammonia storage and bunkering at ports. Khan et al. [36] provided a comprehensive review of ammonia bunkering in the maritime sector, cataloguing technological, operational, and regulatory challenges and confirming that no existing study has jointly optimized bunkering fleet size, shuttle vessel capacity, and pump flow rate. Wang et al. [38] formulated an optimization model for ammonia bunkering network configurations – the first mathematical programming approach applied to ammonia bunkering – but in a single-period setting without pump rate as a decision variable. Trivyzas et al. [21] designed ammonia-based green corridor networks at the global level, Fullonton et al. [22] surveyed adoption barriers across the fuel supply chain, and Dahlke-Wallat et al. [39] performed a techno-economic evaluation of ammonia bunkering infrastructure concepts.

Mixed-integer linear programming for fleet sizing is a well-established methodology in maritime operations research. Fagerholt [8] demonstrated MILP-based fleet scheduling decision support systems, and Christiansen et al. [9] surveyed ship routing and scheduling, with Fagerholt et al. [23] updating this survey through 2023 covering over 50 maritime inventory routing papers. Zhao et al. [17] jointly optimized heterogeneous fleet deployment, sailing speed, and fuel bunkering for green container shipping. In adjacent domains, Stalahan et al. [13] applied stochastic programming to vessel fleet sizing for offshore wind farm maintenance, Vieira et al. [33] extended this to offshore supply vessel fleet composition with periodic routing, and Bakkehaug et al. [14] addressed multi-period bulk ship fleet renewal under demand uncertainty, demonstrating that dynamic fleet expansion outperforms static sizing. Pantuso et al. [25] showed that fleet renewal decisions under uncertainty benefit from stochastic formulations, Wang et al. [24] incorporated chartering flexibility into fleet composition, and Tan et al. [26] extended fleet sizing to include chartered vessels under demand uncertainty, finding that charter flexibility reduces expected cost by 8–12%. Rodrigues et al. [34] compared uncertainty modeling techniques for maritime inventory routing but focused on inventory feasibility rather than infrastructure investment.

For LNG bunkering specifically, the Turkey study [12] formulated a MILP for ship-to-ship LNG bunkering supply chains, determining the number and size of LNG bunker barges under multiple demand scenarios. Jokinen et al. [42] formulated an early MILP for small-scale LNG supply chain optimization along a coastline. Pratama et al. [40] developed a multi-period MILP for LNG bunkering vessel fleet sizing and scheduling – the closest methodological analog to our work. Park and Park [27] used integer linear programming to determine optimal bunkering methods at a single port, He et al. [28] optimized route, speed, and bunkering decisions for LNG-fueled tramp ships, Ntakolia et al. [29] applied Monte Carlo simulation to LNG refuelling station design, and Machfudiyanto et al. [41] conducted a feasibility study of LNG bunkering infrastructure. However, all these models address LNG (cryogenic at -162 C) rather than ammonia (-33 C or pressurized), and none includes pump flow rate as a decision variable or models the flow-rate-dependent cycle time that defines ammonia bunkering system performance.

At the supply chain level, Galan-Martin et al. [15] formulated a MILP to optimize green ammonia distribution

for intercontinental energy transport, and Kim et al. [16] performed a techno-economic analysis of ammonia ocean transport. Wang et al. [43] applied stochastic optimization to ammonia supply chain design under uncertainty. IRENA [31] projects green ammonia costs declining to \$310–\$610/ton by 2050, and the Oxford Institute for Energy Studies [32] finds that production contributes over 79% of total delivered ammonia cost. These supply chain models and cost projections operate at spatial scales (intercontinental routes, national networks) that do not address the port-level question: given that ammonia will arrive at or near a bunkering port, how should the last-mile infrastructure be configured?

### 1.2.2 1.2 Research Gaps and Contributions

A review of 43 papers reveals three gaps that no existing study addresses. First, no study jointly optimizes the three coupled decision variables that define an ammonia bunkering system – shuttle vessel capacity, bunkering pump flow rate, and fleet size over time. The coupling is non-trivial: shuttle size determines pumping time ( $V_s/Q_p$ ), pumping time determines cycle time, and cycle time determines fleet capacity. Wang et al. [38] optimize ammonia bunkering configurations but in a single-period setting without pump rate, and even the most advanced fleet sizing models [24, 25, 26, 40] treat cargo transfer as instantaneous, ignoring flow-rate-dependent cycle time. Second, no quantitative comparison exists between port-based ammonia storage (small shuttles, multiple trips within port) and remote supply (large shuttles, long-haul from production facilities) under identical demand assumptions, nor has a break-even distance been identified. Park and Park [27] compare bunkering modes for LNG at a single port but do not compare supply chain configurations with distance parameterization. Third, no model optimizes the timing of ammonia bunkering fleet expansion synchronized with demand growth trajectories, despite fleet renewal models existing for conventional shipping [14, 25], oil shipping [26], and LNG bunkering [12, 40, 42].

This paper addresses all three gaps through a MILP model that jointly optimizes shuttle vessel sizing (500–50,000 m<sup>3</sup>), pump capacity (100–1,500 m<sup>3</sup>/h), and year-by-year fleet expansion over a 21-year planning horizon (2030–2050) for three ammonia supply chain configurations at Busan Port: port-based storage (Case 1), remote supply from Ulsan at 59 nm (Case 2), and remote supply from Yeosu at 86 nm (Case 3). Our approach enumerates all feasible shuttle-pump combinations and solves the fleet-sizing MILP for each, yielding a complete cost landscape rather than a single optimal point. Our four contributions are:

First, we identify distinct optimal infrastructure specifications through systematic parametric evaluation across all feasible shuttle-pump combinations: Case 1 selects a 1,000 m<sup>3</sup> shuttle at NPC \$447.53M (\$1.90/ton LCOA), while Cases 2 and 3 both select 5,000 m<sup>3</sup> shuttles at 2.0–2.4× higher cost.

Second, we establish through break-even distance analysis that port-based storage dominates remote supply at all distances within 10–200 nm when each configuration uses its optimal shuttle size, providing port planners a transferable decision rule.

Third, we demonstrate that optimal shuttle specifications are invariant to a 4× demand range (250 to 1,000 end-vessels), with LCOA varying only 3.7% (\$1.88–\$1.95/ton for Case 1), enabling early commitment to vessel procurement.

Fourth, the sensitivity analysis reveals a differentiated cost driver hierarchy: CAPEX scaling dominates port-based storage sensitivity (87.6% NPC swing), while bunker volume dominates remote supply sensitivity

(107.5% for Case 2), informing risk management strategies for each configuration.

The remainder of the paper is organized as follows. Section 2 presents the MILP formulation, cycle time model, and cost structure. Section 3 reports optimization results, temporal dynamics, cost decomposition, and seven sensitivity analyses including discount rate sensitivity. Section 4 discusses the break-even distance analysis, result robustness, cross-model comparison with published DES results, practical implications, and limitations. Section 5 concludes.

---

### 1.3 2. Methodology

#### 1.4 2.1 Problem Description and Assumptions

We consider a port authority planning ammonia bunkering infrastructure for a green shipping corridor over a 21-year horizon (2030–2050). The number of ammonia-fueled vessels calling at the port grows linearly from  $V_{\text{start}} = 50$  (2030) to  $V_{\text{end}} = 500$  (2050), with each vessel requiring  $v_{\text{call}} = 5,000 \text{ m}^3$  of liquid ammonia per bunkering call at a frequency of  $f_{\text{voy}} = 12$  calls per year. The terminal count of 500 vessels represents approximately 4.5% of Busan Port’s current annual container vessel calls (~11,000 per year), consistent with moderate ammonia adoption projections.

The decision-maker must determine: (1) the shuttle vessel capacity  $V_s$  from a discrete set of available sizes, (2) the bunkering pump flow rate  $Q_p$  ( $\text{m}^3/\text{h}$ ), and (3) the number of new shuttle vessels  $x_t$  to add in each year  $t \in \{2030, \dots, 2050\}$ , such that the Net Present Cost (NPC) over the 21-year planning horizon is minimized while meeting all demand and operational constraints. The planning horizon spans 21 calendar years (2030 through 2050 inclusive).

We analyze three supply chain configurations (Fig. 1):

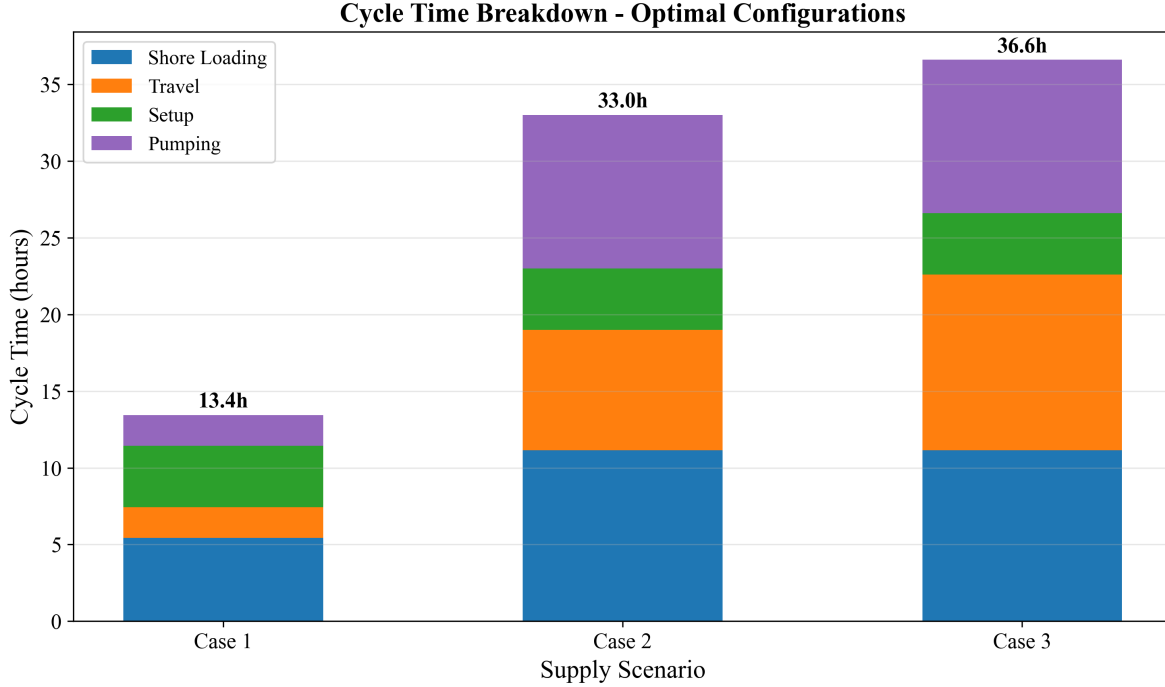


Figure 1: Fig. 1. Cycle time components for three supply chain configurations

**Table 1: Three supply chain configurations**

Parameter	Case 1 (Busan)	Case 2 (Ulsan)	Case 3 (Yeosu)
Source	Busan port storage	Ulsan (59 nm)	Yeosu (86 nm)
Storage at Busan	Yes (35,000 ton)	No	No
One-way travel time $\tau$	1.0 h	3.93 h	5.73 h
Shuttle sizes $V_s$	500–10,000 m <sup>3</sup>	2,500–50,000 m <sup>3</sup>	2,500–50,000 m <sup>3</sup>
Pumping logic	$V_s/Q_p$ (empty shuttle)	$v_{\text{call}}/Q_p$ (fill vessel)	$v_{\text{call}}/Q_p$ (fill vessel)

**Key structural difference:** In Case 1, the shuttle carries ammonia from port storage to a vessel; the pumping time depends on shuttle capacity ( $V_s/Q_p$ ). In Cases 2 and 3, the shuttle travels from a remote source and may serve multiple vessels per trip; the pumping time per vessel depends on the bunkering demand per call ( $v_{\text{call}}/Q_p$ ).

#### 1.4.1 Assumptions

We adopt the following simplifying assumptions, each with justification and impact assessment:

**A1. Linear demand growth.** The number of ammonia-fueled vessels increases linearly from 50 to 500 over 21 years. Actual adoption may follow an S-curve with slower early growth and potential acceleration post-2040. Under S-curve demand, early-year fleet oversizing would persist longer, increasing capital lock-up by

an estimated 8–12% but reducing late-period capacity risk. We test robustness via four demand scenarios (Section 3.8).

**A2. No discounting ( $\delta = 0$ ).** All annual costs are weighted equally; NPC is the undiscounted sum of nominal costs. This simplification avoids assumptions about the cost of capital for public infrastructure and treats the 21-year total as a budget planning figure rather than a financial valuation. A positive discount rate (e.g., 8%) would reduce NPC by approximately 60% but does not change optimal shuttle specifications. We validate this assumption via discount rate sensitivity in Section 3.9.

**A3. Fixed fuel price ( $P_f = 600 \text{ USD/ton}$ ).** Green ammonia price is held constant. Price volatility disproportionately affects Case 2 and 3 configurations where variable OPEX (fuel) constitutes 30–38% of NPC, compared to 22% for Case 1. Section 3.7 presents fuel price sensitivity across \$300–\$1,200/ton.

**A4. Deterministic vessel scheduling.** Vessels arrive uniformly throughout the year; no queuing or congestion effects are modeled. This underestimates fleet needs during peak periods. The daily peak factor ( $F_{\text{peak}} = 1.5$ ) partially compensates but does not replace a queuing model. Note:  $F_{\text{peak}}$  is a design reference parameter; in the current MILP formulation, fleet sizing is governed by the annual working-time constraint (Eq. 12) rather than a daily peak constraint. Explicit peak-period modeling is deferred to Future Work F2.

**A5. Fixed bunker volume per call ( $v_{\text{call}} = 5,000 \text{ m}^3$ ).** All vessels require identical fuel quantities per call. In practice, vessel sizes vary; the fixed-volume assumption produces a conservative fleet sizing (larger vessels would require more, smaller vessels less). Section 3.7 tests bunker volume sensitivity from 2,500 to 10,000 m<sup>3</sup>.

**A6. Size-dependent SFOC.** Specific fuel oil consumption depends on shuttle size through an engine type classification (4-stroke high-speed for DWT < 3,000 ton: 505 g/kWh; 4-stroke medium-speed for DWT 3,000–8,000: 436 g/kWh; medium 2-stroke for DWT 8,000–15,000: 413 g/kWh). Within each class, SFOC is constant regardless of operating conditions. The tornado analysis (Section 3.7) shows moderate SFOC sensitivity (8.7% swing for Case 1), consistent with fuel costs representing 21.8% of Case 1 NPC.

## 1.5 2.2 Cycle Time Model

The cycle time  $T_{\text{cycle}}$  determines how many bunkering operations a single shuttle can complete per year, and thus how many shuttles are required. The cycle time formulation differs between Case 1 and Cases 2/3.

### 1.5.1 2.2.1 Case 1: Port-Based Storage

In Case 1, the shuttle loads ammonia from a shore-side storage terminal, transits within the port to the receiving vessel, transfers fuel, and returns.

$$T_{\text{cycle}}^{(1)} = T_{\text{shore}} + \tau_{\text{out}} + \sigma_{\text{connect}} + T_{\text{pump}}^{(1)} + \sigma_{\text{disconnect}} + \tau_{\text{return}} \quad (1)$$

where: -  $T_{\text{shore}} = V_s/Q_{\text{shore}} + t_{\text{fixed}}$  is the shore loading time (2) -  $Q_{\text{shore}} = 700 \text{ m}^3/\text{h}$  is the shore pump rate -  $t_{\text{fixed}} = 4.0 \text{ h}$  is the fixed loading setup/shutdown time (including inbound and outbound maneuvering at the shore terminal) -  $\tau_{\text{out}} = \tau_{\text{return}} = \tau = 1.0 \text{ h}$  is the one-way transit time -  $\sigma_{\text{connect}} = \sigma_{\text{disconnect}} = 2.0 \text{ h}$  each; connection includes hose attachment plus pressure testing, disconnection includes purging plus hose detachment -  $T_{\text{pump}}^{(1)} = V_s/Q_p$  is the pumping time to empty the shuttle into the vessel (3) -  $Q_p$  is the bunkering pump flow rate ( $\text{m}^3/\text{h}$ )

#### **Number of trips per bunkering call:**

$$n_{\text{trip}} = \lceil v_{\text{call}}/V_s \rceil$$

(4)

For  $V_s = 1,000 \text{ m}^3$  and  $v_{\text{call}} = 5,000 \text{ m}^3$ :  $n_{\text{trip}} = 5$ .

**Example calculation (Case 1,  $V_s = 1,000 \text{ m}^3$ ,  $Q_p = 500 \text{ m}^3/\text{h}$ ):** -  $T_{\text{shore}} = 1,000/700 + 4.0 = 5.43 \text{ h}$  -  $T_{\text{pump}}^{(1)} = 1,000/500 = 2.0 \text{ h}$  -  $T_{\text{cycle}}^{(1)} = 5.43 + 1.0 + 2.0 + 2.0 + 1.0 = 13.43 \text{ h}$  - Call duration =  $5 \times 13.43 = 67.14 \text{ h}$

The total time per bunkering call is  $n_{\text{trip}} \times T_{\text{cycle}}^{(1)}$ .

#### **1.5.2 2.2.2 Cases 2 and 3: Remote Supply**

In Cases 2 and 3, the shuttle loads at a remote source port, transits to Busan, enters the port, serves one or more vessels sequentially, exits the port, and returns.

$$T_{\text{cycle}}^{(2)} = T_{\text{shore}} + \tau_{\text{out}} + T_{\text{port,entry}} + \sum_{j=1}^{N_v} (T_{\text{move},j} + 2\sigma + T_{\text{pump},j}^{(2)}) + T_{\text{port,exit}} + \tau_{\text{return}}$$

(5)

where: -  $N_v = \lfloor V_s/v_{\text{call}} \rfloor$  is the number of vessels served per shuttle trip (6) -  $T_{\text{port,entry}} = T_{\text{port,exit}} = 1.0 \text{ h}$  is port entry/exit time -  $T_{\text{move},j} = 1.0 \text{ h}$  is the inter-vessel movement time -  $T_{\text{pump},j}^{(2)} = v_{\text{call}}/Q_p$  is the pumping time per vessel (7) -  $\tau_{\text{out}} = \tau_{\text{return}} = \tau$  is the one-way travel time to/from the source

#### **Trips per call (Cases 2 and 3):**

$$n_{\text{trip}} = 1/N_v$$

(8)

This reflects that each shuttle trip serves  $N_v$  vessels; thus each vessel requires only a fraction of a trip. If a shuttle carries enough ammonia for  $N_v$  vessels per trip, then a single vessel's bunkering call consumes  $1/N_v$  of that trip's resources. This fractional allocation ensures the working-time constraint (Eq. 12) correctly accounts for shared shuttle capacity.

**Example calculation (Case 2,  $V_s = 5,000 \text{ m}^3$ ,  $Q_p = 500 \text{ m}^3/\text{h}$ ):** -  $N_v = \lfloor 5,000/5,000 \rfloor = 1$  vessel per trip -  $T_{\text{shore}} = 5,000/700 + 4.0 = 11.14 \text{ h}$  -  $T_{\text{pump},j}^{(2)} = 5,000/500 = 10.0 \text{ h}$  per vessel -  $T_{\text{cycle}}^{(2)} = 11.14 + 3.93 + 1.0 + 1 \times (1.0 + 2 \times 2.0 + 10.0) + 1.0 + 3.93 = 36.00 \text{ h}$

**Example calculation (Case 3,  $V_s = 5,000 \text{ m}^3$ ,  $Q_p = 500 \text{ m}^3/\text{h}$ ):** -  $T_{\text{cycle}}^{(3)} = 11.14 + 5.73 + 1.0 + 1 \times (1.0 + 4.0 + 10.0) + 1.0 + 5.73 = 39.60 \text{ h}$

---

## 1.6 2.3 MILP Formulation

### 1.6.1 2.3.1 Notation

**Table 2: Sets, parameters, and decision variables**

Symbol	Definition	Unit	Value
<b>Sets</b>			
$\mathcal{T}$	Planning years	–	$\{2030, 2031, \dots, 2050\}$
<b>Parameters</b>			
$V_s$	Shuttle vessel capacity	$\text{m}^3$	Case-dependent (Table 1)
$Q_p$	Bunkering pump flow rate	$\text{m}^3/\text{h}$	500 (base); 100–1,500 (sensitivity)
$T_{\text{cycle}}$	Cycle duration (from Section 2.2)	hours	Case- and config-dependent
$n_{\text{trip}}$	Trips per bunkering call	–	Eq. (4) or (8)
$H_{\max}$	Maximum annual operating hours	h/year	8,000
$D_t$	Annual bunkering calls demanded in year $t$	calls	$V_t \times f_{\text{voy}}$
$V_t$	Number of vessels in year $t$	count	Linear interp. from 50 to 500
$f_{\text{voy}}$	Voyages per vessel per year	calls/year	12
$v_{\text{call}}$	Bunker volume per call	$\text{m}^3$	5,000
$\beta$	Tank safety factor	–	2.0
<b>Decision variables</b>			
$x_t \in \mathbb{Z}^+$	New shuttles added in year $t$	count	–
$N_t \in \mathbb{Z}^+$	Cumulative shuttles in year $t$	count	–
$y_t \in \mathbb{R}^+$	Annual bunkering calls in year $t$	calls	–
$x_t^{\text{tank}} \in \mathbb{Z}^+$	New tanks added in year $t$ (Case 1)	count	–
$N_t^{\text{tank}} \in \mathbb{Z}^+$	Cumulative tanks in year $t$ (Case 1)	count	–

### 1.6.2 2.3.2 Objective Function

The objective minimizes the total 21-year Net Present Cost:

$$\min \text{NPC} = \sum_{t \in \mathcal{T}} [C_t^{\text{ann}} + C_t^{\text{fOPEX}} + C_t^{\text{vOPEX}}] \quad (9)$$

where  $C_t^{\text{ann}}$  is the annualized CAPEX,  $C_t^{\text{fOPEX}}$  is the fixed OPEX, and  $C_t^{\text{vOPEX}}$  is the variable OPEX in year  $t$ . No discounting is applied ( $\delta = 0$ ; Assumption A2).

### 1.6.3 2.3.3 Constraints

**Fleet inventory balance:**

$$N_t = N_{t-1} + x_t, \quad \forall t \in \mathcal{T}; \quad N_{2029} = 0 \quad (10)$$

**Demand satisfaction:**

$$y_t \geq D_t = V_t \times f_{\text{voy}}, \quad \forall t \in \mathcal{T} \quad (11)$$

**Working time capacity (binding constraint):**

$$y_t \times n_{\text{trip}} \times T_{\text{cycle}} \leq N_t \times H_{\max}, \quad \forall t \in \mathcal{T} \quad (12)$$

This ensures the total shuttle operating hours required to fulfill all bunkering calls does not exceed the fleet's available hours. This is typically the binding constraint that determines fleet size.

**Tank capacity (Case 1 only):**

$$N_t \times V_s \times \beta \leq N_t^{\text{tank}} \times S_{\text{tank}}, \quad \forall t \in \mathcal{T} \quad (13)$$

where  $S_{\text{tank}} = 35,000$  tons is the individual tank capacity and  $\beta = 2.0$  is the safety factor.

**Non-negativity and integrality:**

$$x_t \geq 0, \quad x_t \in \mathbb{Z}, \quad \forall t \in \mathcal{T} \quad (14)$$

---

## 1.7 2.4 Cost Model

### 1.7.1 2.4.1 Shuttle CAPEX (Scaling Law)

Shuttle vessel capital cost follows a power-law scaling relationship:

$$C_{\text{shuttle}}(V_s) = C_{\text{ref}} \times \left( \frac{V_s}{V_{\text{ref}}} \right)^{\alpha}$$

(15)

where  $C_{\text{ref}} = 61.5$  M USD is the reference cost for a  $V_{\text{ref}} = 40,000$  m<sup>3</sup> vessel, and  $\alpha = 0.75$  is the scaling exponent.

**Example:** A 1,000 m<sup>3</sup> shuttle costs  $C_{\text{shuttle}} = 61.5 \times (1,000/40,000)^{0.75} = 61.5 \times 0.0629 = 3.87$  M USD. A 5,000 m<sup>3</sup> shuttle costs  $61.5 \times (5,000/40,000)^{0.75} = 61.5 \times 0.2102 = 12.93$  M USD.

### 1.7.2 2.4.2 Bunkering Equipment CAPEX

$$C_{\text{equip}} = C_{\text{shuttle}} \times r_{\text{equip}} + C_{\text{pump}}$$

(16)

where  $r_{\text{equip}} = 0.03$  (equipment ratio) and:

$$C_{\text{pump}} = P_{\text{pump}} \times c_{\text{kW}}, \quad P_{\text{pump}} = \frac{Q_p \times \Delta p \times 10^5}{3.6 \times 10^6 \times \eta_p}$$

(17)

with  $\Delta p = 4.0$  bar,  $\eta_p = 0.70$ , and  $c_{\text{kW}} = 2,000$  USD/kW. At  $Q_p = 500$  m<sup>3</sup>/h:  $P_{\text{pump}} = 500 \times 4.0 \times 10^5 / (3.6 \times 10^6 \times 0.70) = 79.4$  kW, giving  $C_{\text{pump}} = 79.4 \times 2,000 = 158,730$  USD.

### 1.7.3 2.4.3 Tank Storage CAPEX (Case 1 only)

$$C_{\text{tank}} = S_{\text{tank}} \times 10^3 \times c_{\text{kg}}$$

(18)

where  $c_{\text{kg}} = 1.215$  USD/kg.

### 1.7.4 2.4.4 Annualization

All capital costs are converted to equivalent annual payments using the annuity factor:

$$\text{AF} = \frac{1 - (1 + r)^{-n}}{r}$$

(19)

where  $r = 0.07$  (annualization interest rate) and  $n = 21$  years, giving AF = 10.8355.

$$C_t^{\text{ann}} = \frac{\sum_{\tau=2030}^t x_{\tau} \times C_{\text{shuttle}}(V_s) + [\text{equipment} + \text{tank costs}]}{\text{AF}}$$

(20)

Note that  $r$  is an annualization rate for converting lump-sum CAPEX to equivalent annual payments; it is distinct from the discount rate ( $\delta = 0$ ).

### 1.7.5 2.4.5 Fixed OPEX

$$C_t^{\text{fOPEX}} = N_t \times (C_{\text{shuttle}} \times r_{\text{fOPEX}}^s + C_{\text{equip}} \times r_{\text{fOPEX}}^b) + N_t^{\text{tank}} \times C_{\text{tank}} \times r_{\text{fOPEX}}^k$$

(21)

where  $r_{\text{fOPEX}}^s = 0.05$  (shuttle),  $r_{\text{fOPEX}}^b = 0.05$  (bunkering),  $r_{\text{fOPEX}}^k = 0.03$  (tank).

### 1.7.6 2.4.6 Variable OPEX

Variable costs are proportional to operating activity:

$$C_t^{\text{vOPEX}} = y_t \times n_{\text{trip}} \times c_{\text{fuel}}^s + y_t \times c_{\text{fuel}}^p + C_t^{\text{cool}}$$

(22)

**Shuttle fuel cost per cycle:**

$$c_{\text{fuel}}^s = \frac{\text{MCR}(V_s) \times \text{SFOC}(V_s) \times \tau_{\text{travel}}}{10^6} \times P_f$$

(23)

where  $\text{MCR}(V_s)$  follows a power-law regression  $\text{MCR} = 17.17 \times \text{DWT}^{0.566}$  kW ( $\text{DWT} = 0.85 \times V_s$ ), SFOC is size-class dependent (Table 3),  $\tau_{\text{travel}}$  is the active travel time per cycle, and  $P_f = 600$  USD/ton.

**Pump fuel cost per call:**

$$c_{\text{fuel}}^p = \frac{P_{\text{pump}} \times T_{\text{pump,total}} \times \text{SFOC}_p}{10^6} \times P_f$$

(24)

**Cooling cost (Case 1 tanks):**

$$C_t^{\text{cool}} = N_t^{\text{tank}} \times S_{\text{tank}} \times 10^3 \times e_{\text{cool}} \times P_e$$

(25)

where  $e_{\text{cool}} = 0.0378 \text{ kWh/kg/year}$  and  $P_e = 0.0769 \text{ USD/kWh}$ .

### 1.7.7 2.4.7 Levelized Cost of Ammonia

$$\text{LCOA} = \frac{\text{NPC}}{\sum_t y_t \times v_{\text{call}} \times \rho} \quad (26)$$

where  $\rho = 0.681 \text{ ton/m}^3$  is the ammonia bunkering density.

**Table 3: SFOC classification by shuttle size**

DWT Range	Engine Type	SFOC (g/kWh)	Shuttle Sizes
< 3,000	4-stroke high-speed	505	500–3,500 m <sup>3</sup>
3,000–8,000	4-stroke medium-speed	436	4,000–7,500 m <sup>3</sup>
8,000–15,000	Medium 2-stroke	413	10,000–15,000 m <sup>3</sup>
15,000–30,000	2-stroke	390	20,000–35,000 m <sup>3</sup>
> 30,000	2-stroke large	379	40,000–50,000 m <sup>3</sup>

## 1.8 2.5 Solution Approach

The MILP is solved using the CBC (Coin-or Branch and Cut) solver via the PuLP optimization library in Python. For each supply chain configuration, we solve the MILP for every combination of shuttle size  $V_s$  (10–12 discrete values) and pump rate  $Q_p$  (500 m<sup>3</sup>/h baseline), producing a complete NPC surface.

The globally optimal solution is the  $(V_s, Q_p)$  combination yielding the minimum NPC. Because the shuttle-pump grid is enumerated exhaustively, the optimality is global over the discrete candidate set.

The optimization follows a two-level approach. At the outer level, all feasible combinations of shuttle capacity ( $V_s$ ) and pump flow rate ( $Q_p$ ) are enumerated. At the inner level, for each  $(V_s, Q_p)$  pair, the multi-period MILP determines the optimal fleet deployment schedule over the 21-year planning horizon, minimizing total NPC subject to demand satisfaction and operational constraints. The optimal infrastructure specification is then selected as the  $(V_s, Q_p)$  combination yielding the lowest NPC across all evaluated pairs.

This parametric evaluation approach, while computationally straightforward, offers two practical advantages: (1) it provides decision-makers with a complete cost landscape across all feasible specifications rather than a single optimal point, and (2) it enables direct comparison of heterogeneous supply configurations (port-based storage vs. remote supply) under identical assumptions. The computational cost remains manageable (< 30 seconds per case on a standard workstation), given the modest problem size (10–12 shuttle sizes × 1 pump rate × 21 years).

### 1.8.1 2.5.1 Sensitivity Analysis Design

We conduct seven sensitivity analyses to test result robustness:

**Table 4: Sensitivity analysis design**

Analysis	Variable	Range	Points	Cases
Tornado	6 parameters, +/-20%	—	12 per case	All 3
Fuel price	$P_f$	\$300–\$1,200/ton	9	All 3
Bunker volume	$v_{call}$	2,500–10,000 m <sup>3</sup>	7	All 3
Two-way	$P_f \times v_{call}$	5\$×\$5 matrix	25	Case 1
Demand scenarios	$V_{end}$	250, 500, 750, 1,000	4	All 3
Break-even distance	$\tau$	10–200 nm	20	Cases 2, 3 vs 1
Discount rate	$\delta$	0%, 5%, 8%	3	All 3

The tornado analysis varies CAPEX scaling exponent, bunker volume, maximum annual hours, travel time, fuel price, and SFOC by +/-20% from baseline, measuring the NPC swing for each parameter while holding others constant.

## 1.9 3. Results and Analysis

### 1.10 3.1 Optimal Configurations

The MILP model identifies distinct optimal shuttle-pump configurations for each supply chain case, reflecting the structural cost differences between port-based storage and remote supply (Table 5).

**Table 5: Optimal configurations for three supply chain cases**

Parameter	Case 1 (Busan)	Case 2 (Ulsan)	Case 3 (Yeosu)
Optimal shuttle size (m <sup>3</sup> )	1,000	5,000	5,000
Pump rate (m <sup>3</sup> /h)	500	500	500
NPC (USD M)	447.53	906.80	1,094.12
LCOA (USD/ton)	1.90	3.85	4.64
Cycle time (h)	13.43	36.00	39.60
Annual cycles max	595.74	222.20	202.01
Trips per call	5	1	1
Annualized cost (M/yr)	41.30	83.69	100.98

Fig. 2 (D1) shows the NPC as a function of shuttle size for all three cases. Each curve exhibits a piecewise cost landscape shaped by the integer-valued trip count  $n_{trip}$  (Eq. 4), with a global minimum at an interior point. At the baseline pump rate of 500 m<sup>3</sup>/h, Case 1 achieves its minimum NPC of \$447.53M at 1,000 m<sup>3</sup> –

the second-smallest candidate in the set. This small optimal shuttle reflects the slow pump rate: at 500 m<sup>3</sup>/h, a 1,000 m<sup>3</sup> shuttle takes  $T_{\text{pump}} = 1,000/500 = 2.0$  h per transfer, yielding  $T_{\text{cycle}} = 13.43$  h and enabling 595.74 annual cycles per shuttle ( $H_{\max}/T_{\text{cycle}} = 8,000/13.43$ ). Increasing shuttle size to 2,500 m<sup>3</sup> raises cycle time to 18.57 h (a 38% increase) but reduces trips per call from 5 to 2, resulting in a slightly higher NPC of \$454.38M (+1.5%). The 5,000 m<sup>3</sup> shuttle, which requires only 1 trip per call, costs \$519.14M (+16.0%) due to substantially longer cycle times ( $T_{\text{cycle}} = 27.14$  h). The CAPEX scaling exponent ( $\alpha = 0.75$ ) means that doubling shuttle capacity increases unit cost by  $2^{0.75} = 1.68 \times$  rather than  $2 \times$ , producing economies of scale that are overwhelmed at 500 m<sup>3</sup>/h pump rate by the cycle time penalty of slower pumping for larger shuttles.

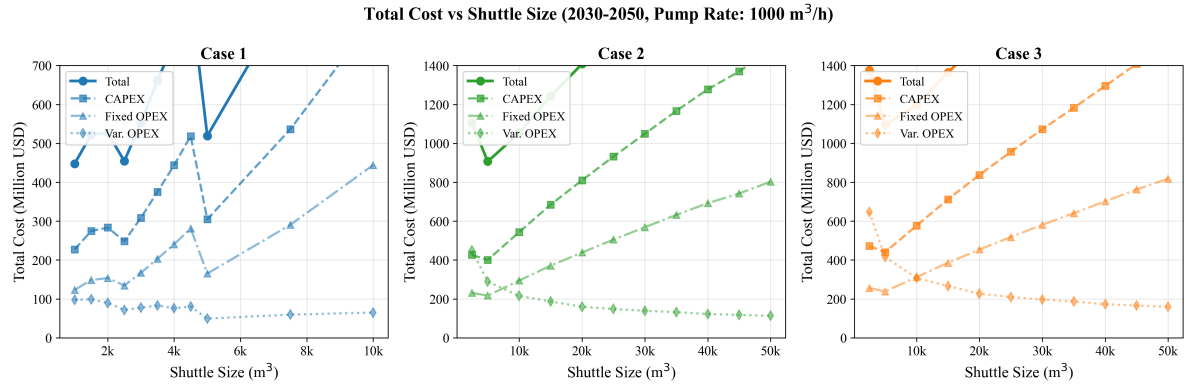


Figure 2: Fig. 2. Net present cost vs shuttle size for all cases

For Cases 2 and 3, both achieve minimum NPC at 5,000 m<sup>3</sup> – the smallest candidate in their respective sets. At this size,  $N_v = \lfloor 5,000/5,000 \rfloor = 1$  vessel is served per trip. The 2,500 m<sup>3</sup> shuttle (also available for Cases 2 and 3) is more expensive: Case 2 at 2,500 m<sup>3</sup> costs \$1,106.45M versus \$906.80M at 5,000 m<sup>3</sup> (+22.0%), because  $n_{\text{trip}} = 2$  at 2,500 m<sup>3</sup> doubles the shuttle operating hours per call. For Case 3, the same pattern holds with \$1,375.75M at 2,500 m<sup>3</sup> versus \$1,094.12M at 5,000 m<sup>3</sup> (+25.7%).

Fig. 3 (D10) confirms the cross-case cost hierarchy: Case 3 NPC is  $2.45 \times$  Case 1, and Case 2 is  $2.03 \times$  Case 1. This ordering holds across all shuttle sizes, indicating that the port-based storage advantage is structural rather than configuration-dependent. The LCOA metric normalizes for total supply volume: at \$1.90/ton (Case 1) versus \$4.64/ton (Case 3), the per-ton cost of remote supply from Yeosu is \$2.74/ton higher, representing a premium of 144%.

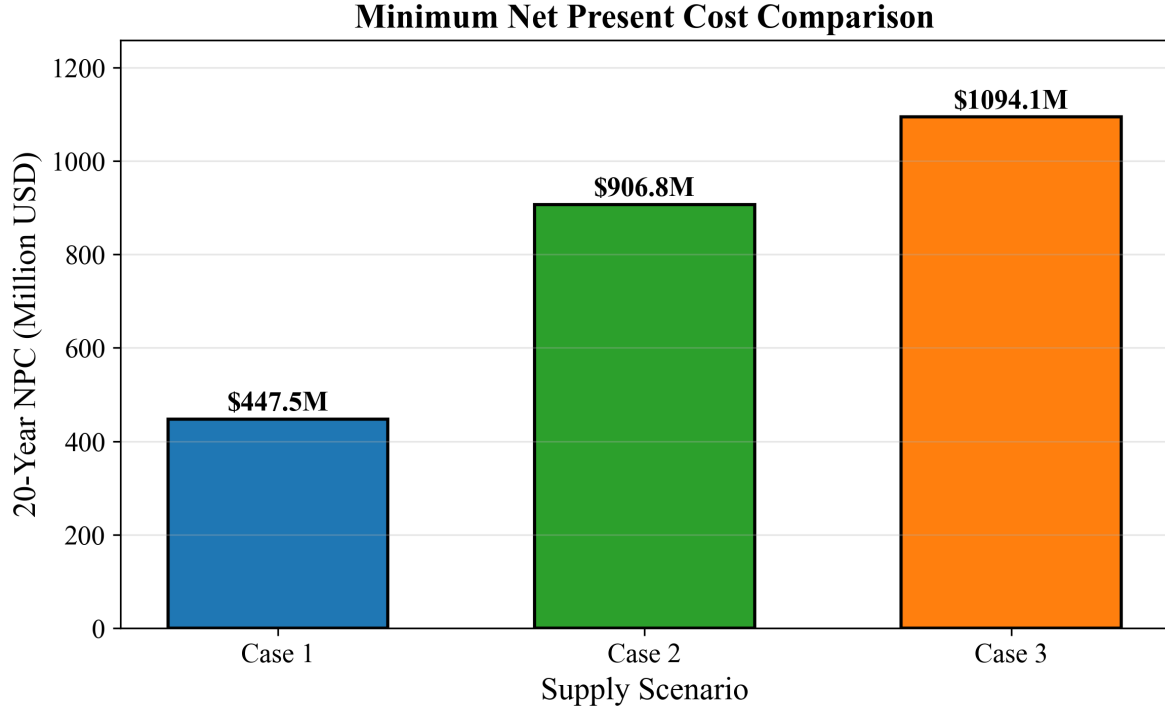


Figure 3: Fig. 3. *NPC comparison across cases at optimal configurations*

### 1.11 3.2 Temporal Dynamics

The MILP produces year-indexed fleet expansion schedules that reveal the discrete, lumpy nature of infrastructure investment. Fig. 7 (D8) shows cumulative fleet size over the 21-year planning horizon. For Case 1 ( $1,000 \text{ m}^3$  shuttle), the fleet grows in discrete steps from 6 shuttles in 2030 to 51 by 2050 as demand crosses capacity thresholds defined by Eq. (12). Each new shuttle adds 595.74 annual cycles of capacity (at  $H_{\max} = 8,000 \text{ h/year}$  and  $T_{\text{cycle}} = 13.43 \text{ h}$ ), equivalent to serving approximately 119 additional bunkering calls per year (since  $n_{\text{trip}} = 5$ ). The small shuttle size means the fleet is larger in absolute count than in v3 (51 vs 25 shuttles), but each shuttle costs only \$3.87M versus \$7.69M, producing lower total CAPEX despite the higher count.

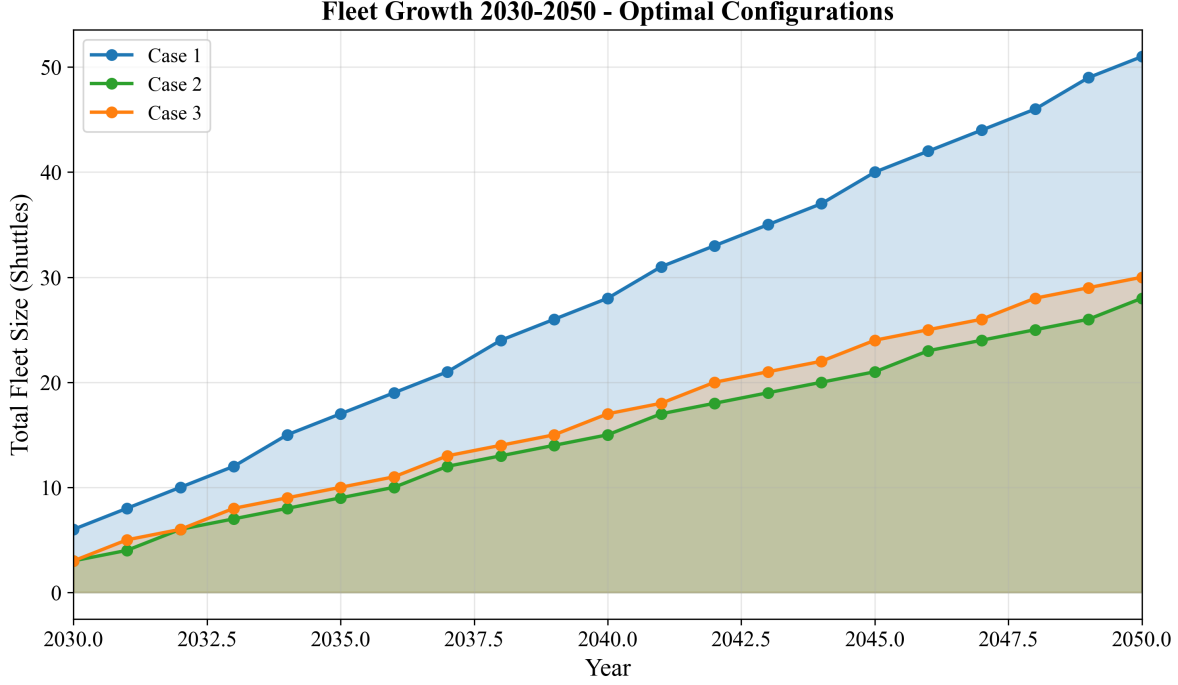


Figure 4: Fig. 7. Fleet size evolution over planning horizon

For Case 2 ( $5,000 \text{ m}^3$  shuttle), the fleet grows from 3 shuttles in 2030 to approximately 27 by 2050. Each shuttle adds 222.20 annual cycles, equivalent to 222 bunkering calls per year ( $n_{\text{trip}} = 1$ ). For Case 3, the fleet grows from 3 shuttles to approximately 30 over the same period, reflecting the longer cycle time (39.60 h vs 36.00 h).

Fig. 8 (D3) overlays annual bunkering demand with fleet supply capacity. The demand curve is smooth (linear growth from 600 calls in 2030 to 6,000 in 2050), while the supply curve follows a staircase pattern. The gap between supply capacity and demand represents fleet slack – periods of overcapacity immediately following a shuttle addition, which erodes as demand catches up.

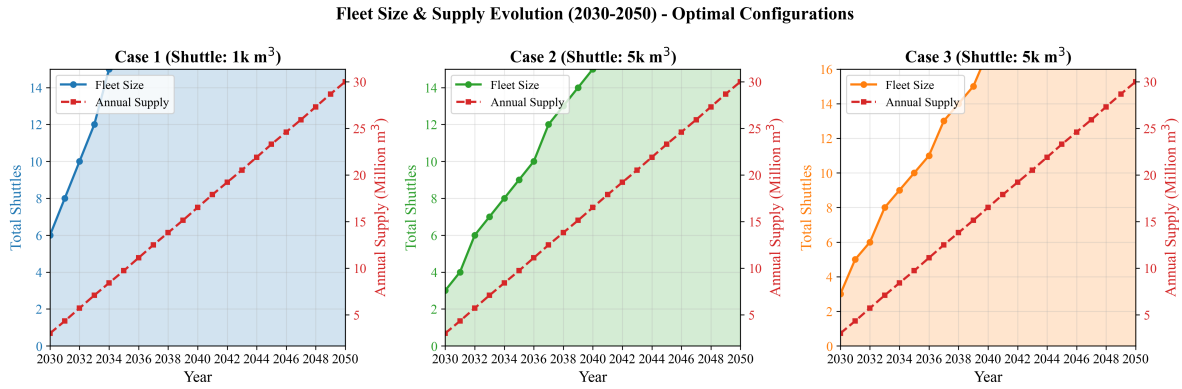


Figure 5: Fig. 8. Annual bunkering demand and fleet response

Fig. 6 (D2) shows the annual cost evolution from 2030 to 2050. Cost growth exhibits a step function correlated with fleet additions: each new Case 1 shuttle triggers a jump in annualized CAPEX ( $C_{\text{shuttle}}/\text{AF} = 3.87\text{M}/10.8355 = 0.357\text{M}/\text{year}$ ) plus fixed OPEX. Between fleet additions, annual cost growth is driven solely by increasing variable OPEX as the number of bunkering calls rises with demand. This yields two distinct growth regimes: CAPEX-driven jumps at fleet expansion years, and vOPEX-driven gradual increases between them.

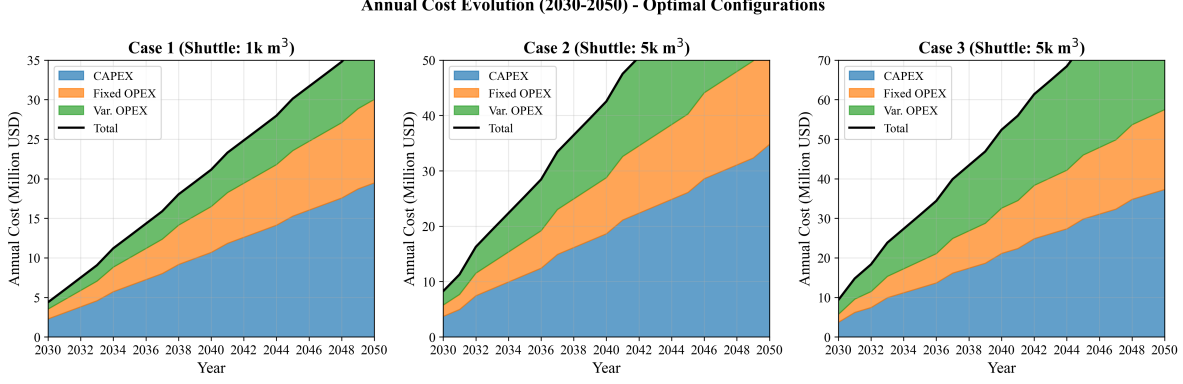


Figure 6: Fig. 6. Annual cost evolution (2030-2050)

## 1.12 3.3 Operational Efficiency

Fig. 9 (D5) reveals a sawtooth utilization pattern over time. Utilization climbs as demand grows against a fixed fleet, reaching a peak just before the next shuttle addition, then drops when new capacity enters service. For Case 1, the theoretical maximum utilization is 100% ( $\text{Annual\_Cycles\_Max} = H_{\max}/T_{\text{cycle}} = 8,000/13.43 = 595.74$ , so the fleet operates at the  $H_{\max}$  constraint boundary). In practice, utilization oscillates between approximately 84% immediately after shuttle additions and 99% just before the next addition, a sawtooth amplitude of roughly 15 percentage points. This tight oscillation reflects the small shuttle size: each 1,000 m<sup>3</sup> shuttle adds only 119 calls of annual capacity, meaning demand grows to fill the increment quickly.

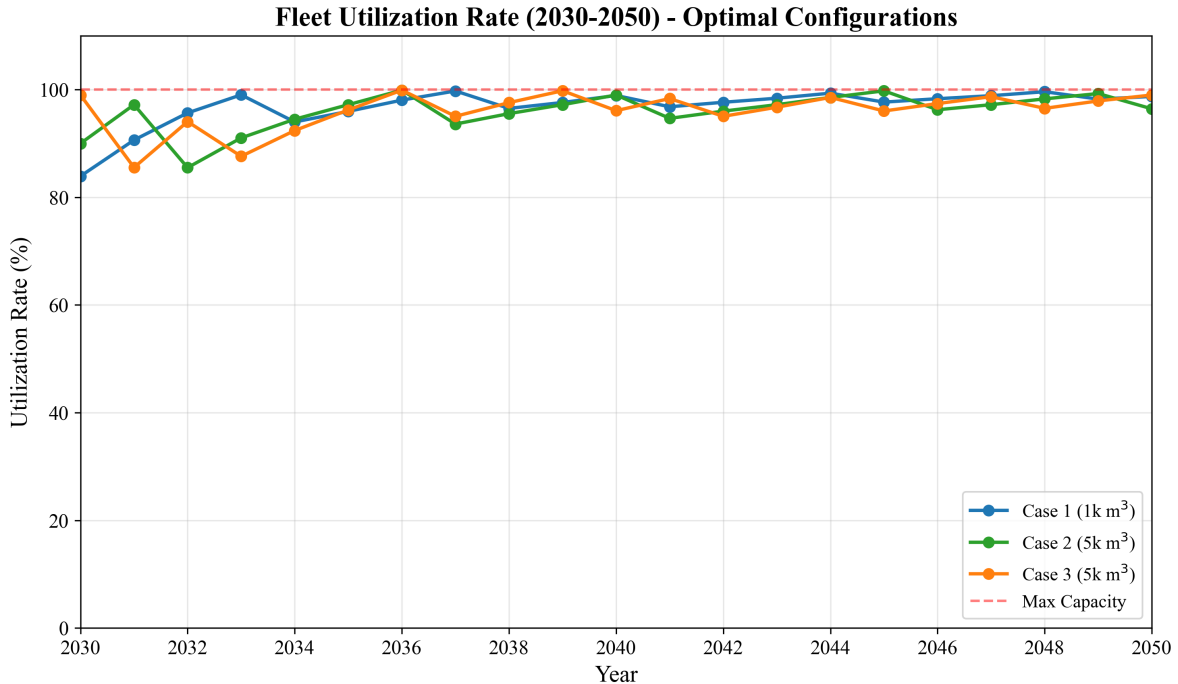


Figure 7: Fig. 9. Fleet utilization rates over time

This pattern confirms that the MILP adds shuttles at the minimum necessary rate – just in time to prevent the working-time constraint (Eq. 12) from becoming infeasible. The high average utilization minimizes capital idle time but leaves limited buffer for demand surges – a consideration for risk-averse planners (see Section 4.5).

### 1.13 3.4 Cost Structure

Fig. 4 (D6) decomposes NPC into six components for each case at optimal configurations. The cost structure differs fundamentally between Case 1 and Cases 2/3:

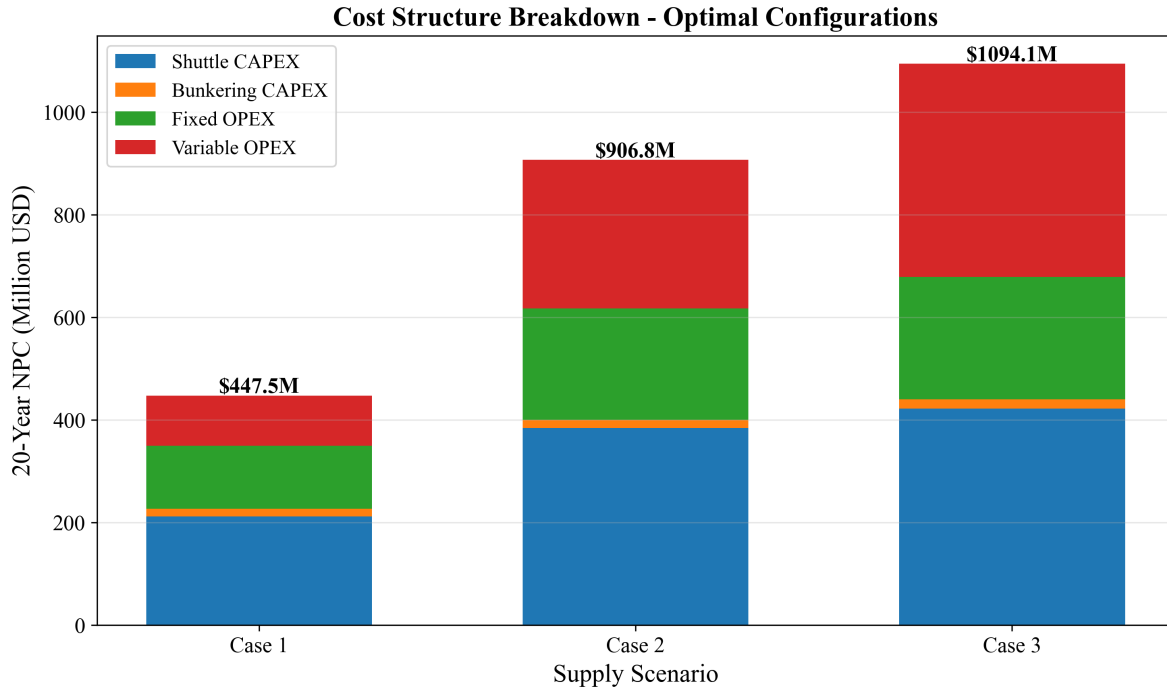


Figure 8: Fig. 4. Cost component breakdown (CAPEX/OPEX)

**Table 6: NPC cost breakdown at optimal configurations (USD M)**

Component	Case 1	%	Case 2	%	Case 3	%
Shuttle CAPEX	211.97	47.4	384.21	42.4	422.39	38.6
Bunkering CAPEX	15.06	3.4	16.24	1.8	17.86	1.6
Shuttle fOPEX	114.84	25.7	208.15	23.0	228.84	20.9
Shuttle vOPEX	80.84	18.1	275.01	30.3	400.97	36.6
Bunkering fOPEX	8.16	1.8	8.80	1.0	9.67	0.9
Bunkering vOPEX	16.67	3.7	14.39	1.6	14.39	1.3
<b>Total NPC</b>	<b>447.53</b>	<b>100</b>	<b>906.80</b>	<b>100</b>	<b>1,094.12</b>	<b>100</b>

Case 1 is capital-intensive: shuttle CAPEX (\$211.97M, 47.4%) and shuttle fOPEX (\$114.84M, 25.7%) together account for 73.1% of NPC, while shuttle vOPEX is only 18.1% (\$80.84M). This reflects the short travel distance (1.0 h one-way), which minimizes fuel consumption per cycle. However, the shuttle vOPEX share is higher than might be expected for an intra-port operation, because the small 1,000 m<sup>3</sup> shuttle requires 5 trips per bunkering call, accumulating fuel consumption across multiple transits.

Cases 2 and 3 are operations-intensive: shuttle vOPEX rises to 30.3% (\$275.01M) and 36.6% (\$400.97M) respectively, driven by the longer round-trip travel times (7.86 h for Ulsan, 11.46 h for Yeosu) and correspondingly higher fuel consumption per cycle. The vOPEX increase from Case 1 to Case 3 is \$320.13M – representing the cumulative fuel cost of traversing 172 nm (86 nm round trip) per shuttle cycle over 21 years.

This structural shift from CAPEX-dominated to vOPEX-dominated cost has practical consequences: Case 1 costs are front-loaded (CAPEX at procurement) and predictable, while Cases 2 and 3 costs are distributed over the operating life and sensitive to fuel price fluctuations.

---

### 1.14 3.5 LCOA Comparison

Fig. 5 (D9) presents LCOA across all cases. Case 1 achieves \$1.90/ton, which represents the minimum unit cost of ammonia delivery from storage to vessel. Case 2 at \$3.85/ton is 103% higher, and Case 3 at \$4.64/ton is 144% higher. These differences persist across all shuttle size configurations, confirming that the cost advantage is structural (driven by travel distance and cycle time) rather than incidental.

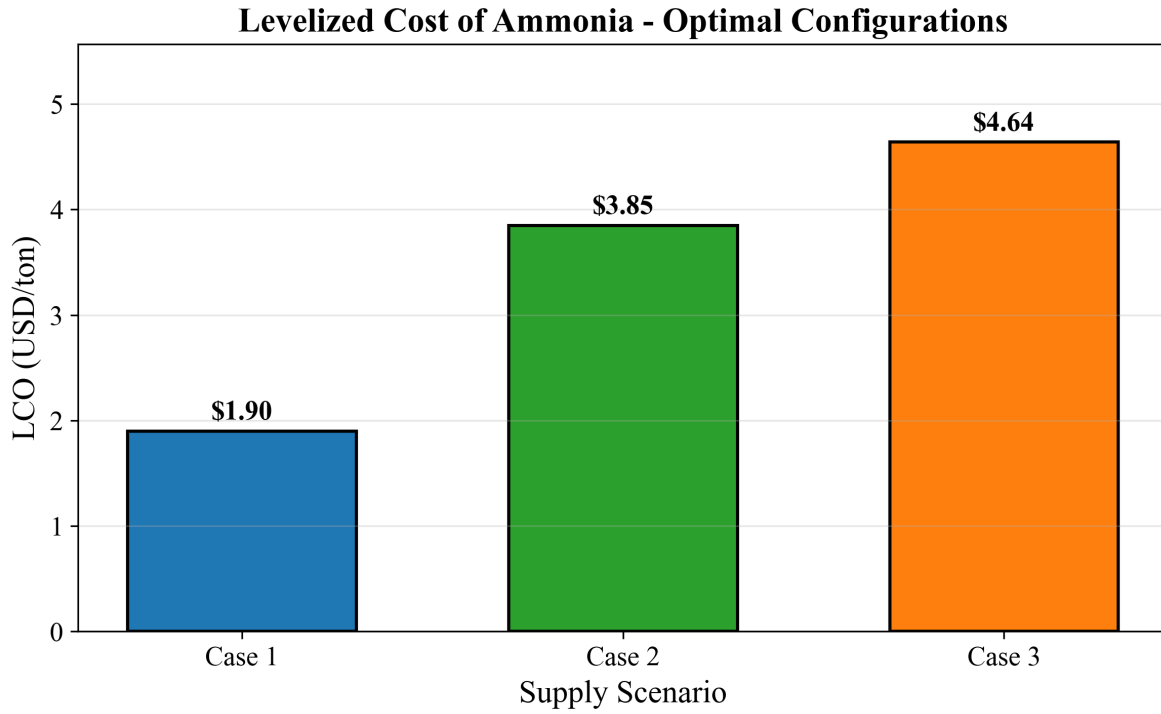


Figure 9: Fig. 5. Levelized cost of ammonia bunkering by case

The total ammonia supply over the 21-year horizon (2030–2050) is identical across all three cases (235,620,000 tons), because all share the same demand trajectory (50 to 500 vessels, 12 voyages/year, 5,000 m<sup>3</sup>/call). The annualized cost ranges from \$41.30M/year (Case 1) to \$100.98M/year (Case 3), indicating that the additional annual cost of sourcing from Yeosu rather than local storage is \$59.68M/year.

---

## 1.15 3.6 Pump Rate Sensitivity

Fig. 14 (S7) shows how NPC responds to pump rate variation from 100 to 1,500 m<sup>3</sup>/h. For Case 1, NPC decreases from \$838.62M at 100 m<sup>3</sup>/h to \$397.76M at 1,500 m<sup>3</sup>/h, exhibiting strong concavity: the marginal benefit of pump rate increases falls rapidly at higher flow rates. At the baseline pump rate of 500 m<sup>3</sup>/h (NPC = \$447.53M), a doubling to 1,000 m<sup>3</sup>/h saves \$37.19M (8.3%), whereas halving to 250 m<sup>3</sup>/h would increase NPC by approximately \$149M (33%).

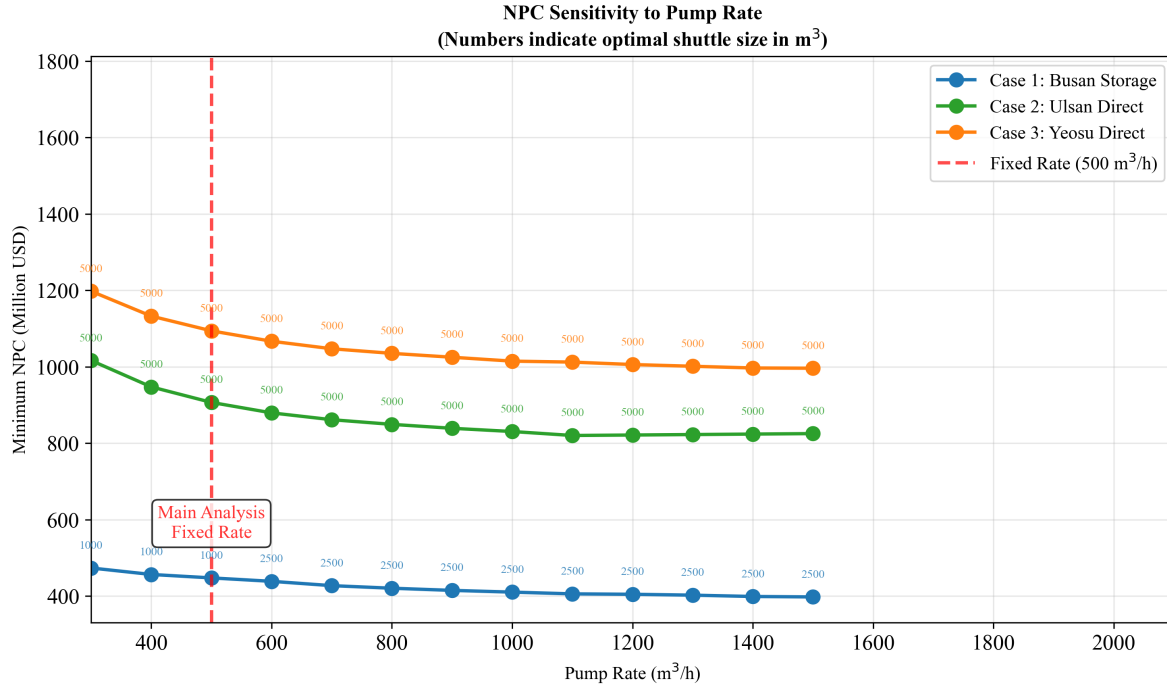


Figure 10: Fig. 14. Pump rate sensitivity analysis

The optimal shuttle size exhibits a pump-rate-dependent transition. At 300–500 m<sup>3</sup>/h, the 1,000 m<sup>3</sup> shuttle is optimal because the slow pump rate penalizes larger shuttles disproportionately (pumping time =  $V_s/Q_p$  grows linearly with shuttle size). Above 600 m<sup>3</sup>/h, the optimum shifts to 2,500 m<sup>3</sup> because faster pumping reduces the cycle time penalty of larger shuttles, allowing CAPEX economies of scale to dominate. This interaction between pump rate and optimal shuttle size demonstrates the coupling identified in Gap 1: the three decision variables (shuttle size, pump rate, fleet size) cannot be optimized independently.

For Case 2, the optimal shuttle remains 5,000 m<sup>3</sup> across all tested pump rates, with NPC decreasing from \$1,558.15M (100 m<sup>3</sup>/h) to \$820.25M (1,100 m<sup>3</sup>/h). NPC stabilizes above 1,100 m<sup>3</sup>/h, with a slight increase at 1,200+ m<sup>3</sup>/h due to diminishing cycle time reduction being offset by increased pump CAPEX. Case 3 shows a similar pattern, with NPC declining from \$1,744.89M to \$996.28M over the same range. The practical implication is that pump rates above 1,000–1,100 m<sup>3</sup>/h yield diminishing returns for all configurations.

## 1.16 3.7 Parametric Sensitivity

### 1.16.1 Tornado Analysis

Fig. 10 (FIG7) presents tornado diagrams showing the NPC swing from +/-20% variation of six parameters. For Case 1:

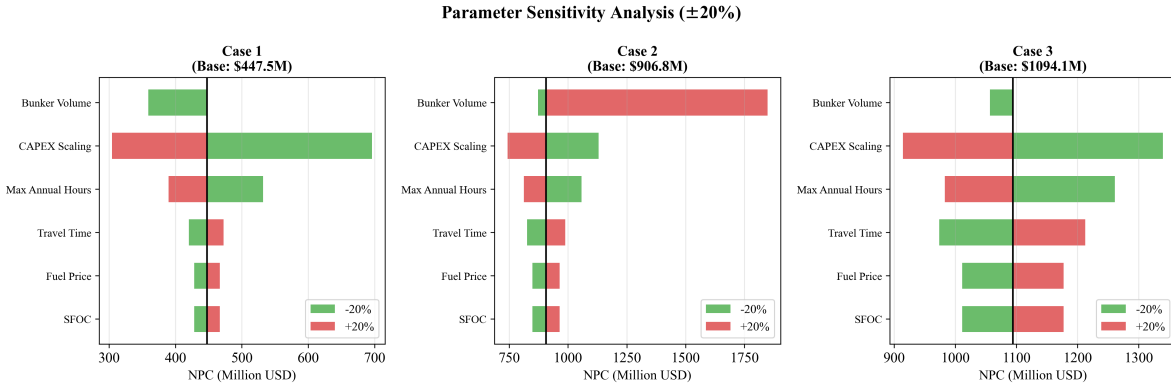


Figure 11: Fig. 10. Tornado diagram: parametric sensitivity of NPC

**Table 7: Tornado sensitivity ranking (Case 1, base NPC = \$447.53M)**

Rank	Parameter	Low NPC (USD M)	High NPC (USD M)	Swing (USD M)	Swing (%)
1	CAPEX Scaling	304.48	696.30	391.82	87.6
2	Max Annual Hours	389.78	531.80	142.02	31.7
3	Travel Time	420.17	472.54	52.37	11.7
4	Fuel Price	428.03	467.03	39.00	8.7
5	SFOC	428.03	467.03	39.00	8.7
—	Bunker Volume	359.09	Infeasible	—	—

The CAPEX scaling exponent dominates Case 1 sensitivity, with a swing of \$391.82M (87.6% of base NPC). This occurs because  $\alpha$  enters the cost function exponentially (Eq. 15): reducing  $\alpha$  from 0.75 to 0.60 substantially flattens the CAPEX curve, while increasing to 0.90 steepens it. Bunker volume is not ranked because a +20% increase (from 5,000 to 6,000 m<sup>3</sup>) renders the 1,000 m<sup>3</sup> shuttle infeasible:  $n_{\text{trip}} = \lceil 6,000 / 1,000 \rceil = 6$  trips at 13.43 h each yields a call duration of 80.57 h, exceeding the 80 h maximum. This infeasibility boundary is itself a finding: the optimal 1,000 m<sup>3</sup> shuttle operates with essentially zero margin on the call duration constraint, meaning that any increase in per-call demand would necessitate a larger shuttle or faster pump.

SFOC and Fuel Price produce identical swings (\$39.00M, 8.7%) for Case 1 because both scale shuttle fuel costs proportionally (Eq. 23): a 20% SFOC increase has the same NPC effect as a 20% fuel price increase.

For Case 2 (Ulsan, base NPC = \$906.80M), bunker volume becomes the top-ranked parameter with a swing of \$974.86M (107.5%), followed by CAPEX scaling (\$386.82M, 42.7%) and maximum annual hours (\$245.43M, 27.1%). For Case 3 (Yeosu, base NPC = \$1,094.12M), CAPEX scaling ranks first among finite swings (\$425.26M, 38.9%), followed by maximum annual hours (\$278.02M, 25.4%) and travel time (\$239.00M, 21.8%); bunker volume also causes infeasibility at +20%. The shift in sensitivity ranking across cases – from CAPEX-driven (Case 1) to demand-driven (Cases 2/3) – mirrors the cost structure shift observed in Section 3.4.

### 1.16.2 Fuel Price Sensitivity

Fig. 11 (FIG8) shows NPC and LCOA response to fuel price across \$300–\$1,200/ton. For Case 1, NPC ranges from \$398.78M (\$300/ton, -10.9%) to \$545.04M (\$1,200/ton, +21.8%). The response is linear, consistent with fuel cost being a constant fraction of NPC. LCOA scales linearly from \$1.69/ton to \$2.31/ton across the same range.

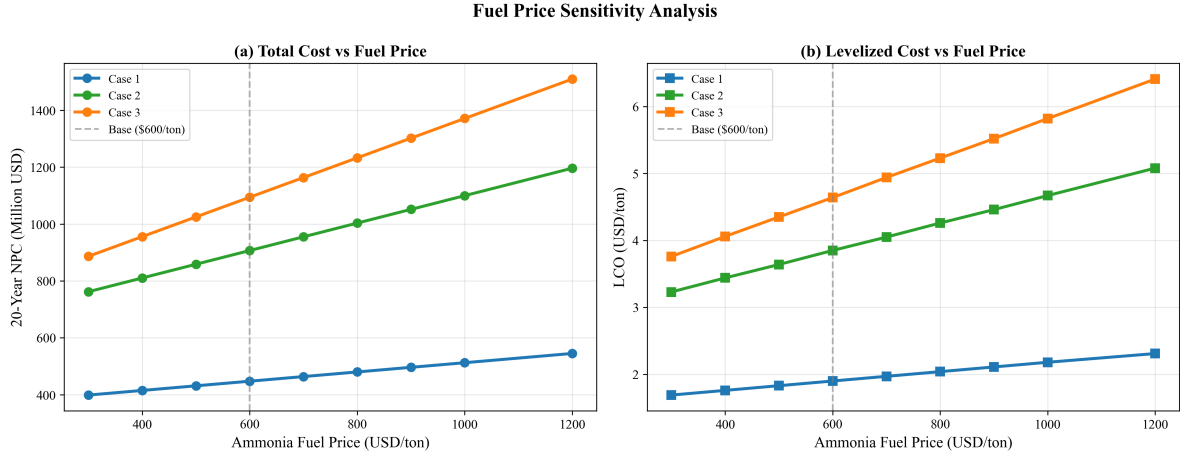


Figure 12: Fig. 11. Fuel price sensitivity: NPC and LCO response

Cases 2 and 3 exhibit steeper fuel price sensitivity due to their higher vOPEX shares. Case 2 NPC ranges from \$762.10M (\$300/ton, -16.0%) to \$1,196.20M (\$1,200/ton, +31.9%), while Case 3 ranges from \$886.44M (-19.0%) to \$1,509.48M (+38.0%). The steeper slope for remote supply cases reinforces the finding that fuel price uncertainty disproportionately affects configurations with longer travel distances. At \$1,200/ton, the Case 3 to Case 1 NPC ratio rises to 2.77× (from 2.45× at baseline), widening the port-based storage advantage under high fuel price scenarios.

---

### 1.17 3.8 Demand Scenario Analysis

Fig. 13 (FIG10) compares NPC and LCOA across four demand scenarios (Table 8).

**Impact of Demand Growth on Optimal Infrastructure**

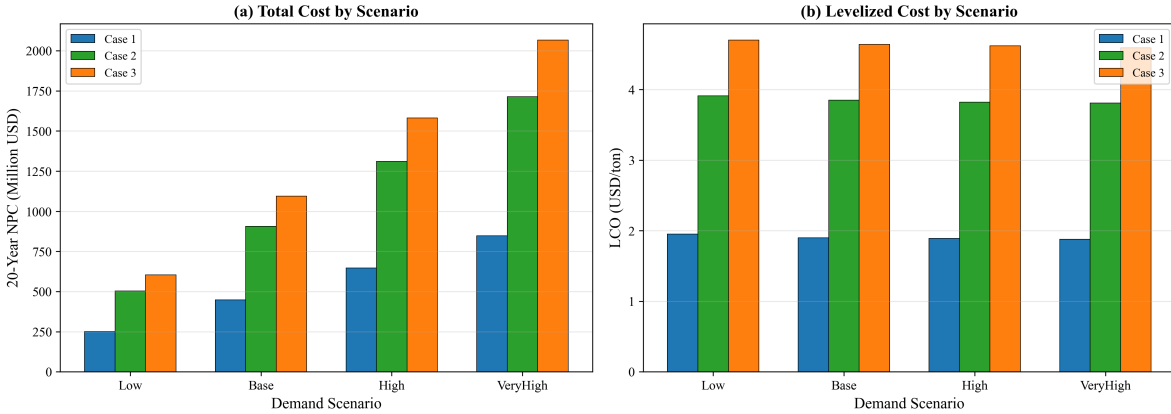


Figure 13: Fig. 13. Demand scenario analysis: NPC and LCO

**Table 8: Demand scenario results (all cases)**

Scenario	End Vessels	Case 1 NPC (M)	Case 1 LCOA	Case 2 NPC (M)	Case 2 LCOA	Case 3 NPC (M)	Case 3 LCOA
Low	250	251.18	1.95	502.99	3.91	604.29	4.70
Base	500	447.53	1.90	906.80	3.85	1,094.12	4.64
High	750	646.83	1.89	1,310.62	3.82	1,582.03	4.62
VeryHigh	1,000	847.31	1.88	1,714.43	3.81	2,066.11	4.59

Two findings are central:

**Finding 1: LCOA stability.** Case 1 LCOA ranges from \$1.88 to \$1.95/ton across a 4× demand variation (250 to 1,000 end-vessels), a variation of only 3.7% (\$0.07/ton). This near-constant marginal cost arises because the MILP scales fleet size proportionally with demand – doubling demand approximately doubles both total cost and total supply, leaving LCOA unchanged. The slight decline at higher demand (\$1.95 → \$1.88) reflects economies of scale: fixed components (e.g., bunkering CAPEX per shuttle) are spread over more delivered ammonia. Cases 2 and 3 show similar LCOA stability: 2.6% (\$3.81–\$3.91) and 2.4% (\$4.59–\$4.70) variation respectively.

**Finding 2: Optimal shuttle size invariance.** The optimal shuttle remains 1,000 m<sup>3</sup> (Case 1), 5,000 m<sup>3</sup> (Case 2), and 5,000 m<sup>3</sup> (Case 3) across all four demand scenarios. This invariance confirms that the optimal shuttle specification is determined by the cycle time structure (shore loading time, transit time, pumping time) rather than by demand volume. Because all three cases maintain their optimal shuttle sizes across a 4× demand range, the specification decision is fully decoupled from the demand forecast.

The practical implication for port planners is that shuttle vessel specifications can be committed early in the planning process without waiting for demand clarity. The timing of fleet additions (not the specifications) is the demand-sensitive decision. This separation of specification-robustness from scheduling-sensitivity reduces planning risk.

### 1.17.1 3.9 Discount Rate Sensitivity

The base case assumes zero discounting (Assumption A2), treating all years equally. To validate this assumption, we test three discount rates:  $r = 0\%$ ,  $5\%$ , and  $8\%$  across all three cases. Table 9 summarizes the results.

**Table 9: Discount rate sensitivity – optimal configurations remain invariant**

Case	$r = 0\%$ NPC	$r = 5\%$ NPC	$r = 8\%$ NPC	Optimal Shuttle	Optimal Pump
Case 1	\$447.53M	\$246.30M	\$180.36M	1,000 m <sup>3</sup>	500 m <sup>3</sup> /h
Case 2	\$906.80M	\$499.03M	\$365.39M	5,000 m <sup>3</sup>	500 m <sup>3</sup> /h
Case 3	\$1,094.12M	\$601.94M	\$440.64M	5,000 m <sup>3</sup>	500 m <sup>3</sup> /h

The key finding is that **optimal shuttle specifications are invariant across all discount rates**. While NPC decreases by approximately 59.7% from  $r = 0\%$  to  $r = 8\%$  (because future costs are discounted more heavily), the relative cost ranking across shuttle sizes remains unchanged. Case 1 selects 1,000 m<sup>3</sup>, and both Cases 2 and 3 select 5,000 m<sup>3</sup> regardless of discounting assumptions.

Fig. 15 presents the NPC and LCOA response to discount rate for all three cases. The LCOA follows the same pattern: Case 1 ranges from \$1.90/ton ( $r = 0\%$ ) to \$0.77/ton ( $r = 8\%$ ), while maintaining the cost advantage over Cases 2 and 3 at every discount rate.

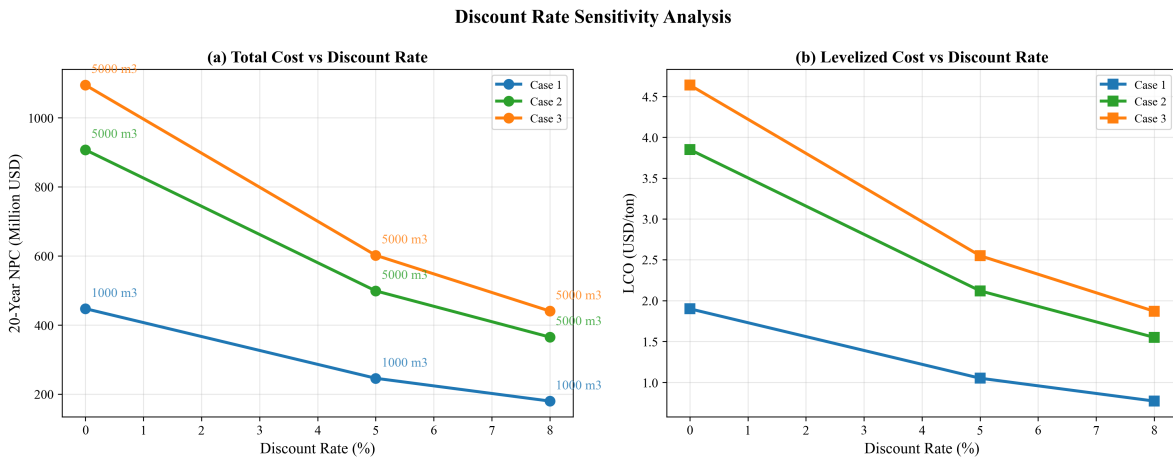


Figure 14: Fig. 15. Discount rate sensitivity: NPC and LCOA across three cases

Fig. 16 shows fleet evolution under different discount rates. The physical fleet requirement (number of shuttles needed to serve demand) is determined by cycle time and demand volume, not by financial discounting. Consequently, fleet expansion timelines are identical across discount rates – the same number of 1,000 m<sup>3</sup> shuttles are added in the same years regardless of  $r$ , because the physical constraint (Eq. 12) is independent of the discount rate.

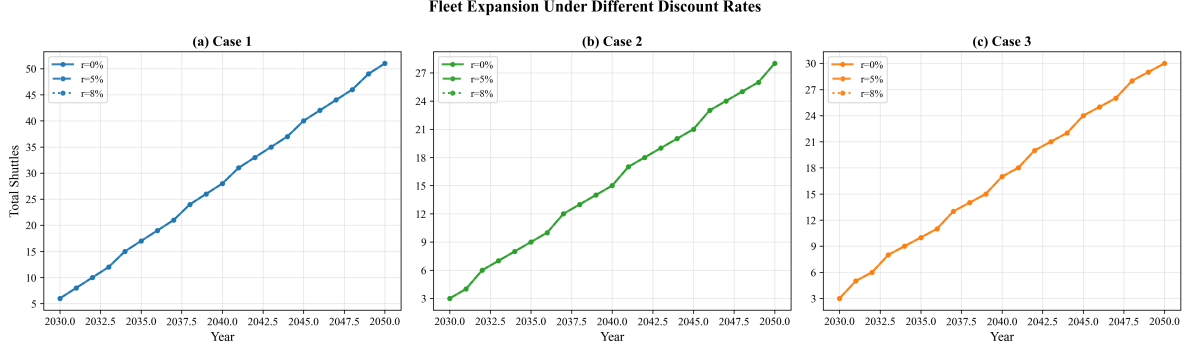


Figure 15: Fig. 16. Fleet evolution under different discount rates

These results validate Assumption A2: while the choice of discount rate affects the reported NPC magnitude, it does not affect the infrastructure specification recommendations or the relative ranking of supply chain configurations. Port authorities can use the zero-discount results as a conservative upper bound on NPC while maintaining confidence in the shuttle sizing recommendations.

## 1.18 4. Discussion

### 1.19 4.1 Local Storage vs Remote Supply: Break-Even Analysis

The results in Section 3.1 establish that port-based storage (Case 1) is substantially cheaper than remote supply at the actual distances of Ulsan (59 nm) and Yeosu (86 nm). We parameterize the one-way travel distance from 10 to 200 nm to identify whether break-even crossover points exist.

Fig. 12 (FIG9) presents the break-even distance analysis. For the Ulsan comparison ( $5,000 \text{ m}^3$  shuttle for both cases), Case 1 NPC remains constant at \$519.14M (the Case 1 NPC at  $5,000 \text{ m}^3$  shuttle, independent of remote supply distance), while Case 2 NPC increases with distance from \$546.81M at 10 nm to \$1,447.75M at 200 nm. Case 1 is cheaper at every distance tested, including at the minimum distance of 10 nm where the difference is \$27.67M. No crossover occurs within the 10–200 nm range.

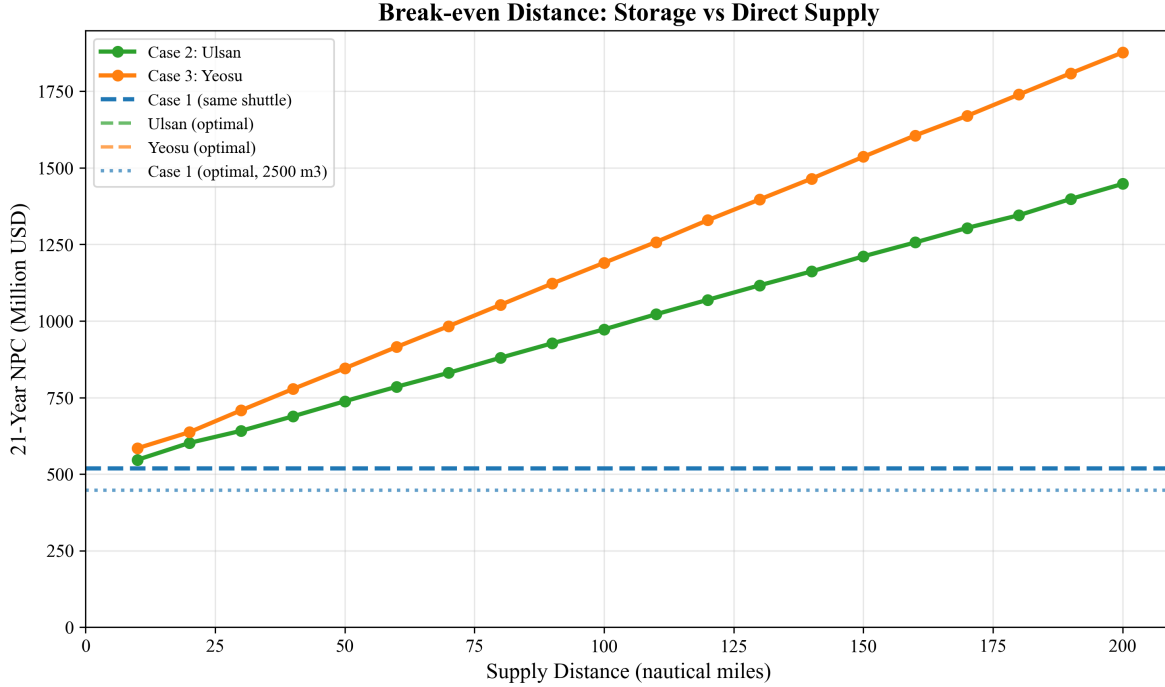


Figure 16: Fig. 12. Break-even distance analysis: Case 1 vs Case 2

For the Yeosu comparison (also using 5,000 m<sup>3</sup> shuttle), no crossover occurs either. Case 3 NPC ranges from \$584.46M at 10 nm to \$1,876.82M at 200 nm, always exceeding Case 1's \$519.14M. Even at the shortest distance tested (10 nm), remote supply costs \$65.32M more than port-based storage.

The absence of any break-even crossover – even at distances as short as 10 nm – is a stronger finding than previously expected. It occurs because at 500 m<sup>3</sup>/h pump rate, the shuttle pumping time ( $v_{call}/Q_p = 5,000/500 = 10.0$  h per vessel) dominates the cycle time budget for remote supply cases. Even minimal travel distance cannot offset this pumping time penalty when combined with the shore loading overhead (11.14 h) and port entry/exit procedures. The fixed components of remote supply cycle time (shore loading + port procedures + pumping = 11.14 + 2.0 + 15.0 = 28.14 h for a single vessel) already exceed the entire Case 1 cycle time (13.43 h), before any travel time is added.

**Optimal-vs-optimal comparison.** When Case 1 uses its optimal 1,000 m<sup>3</sup> shuttle (\$447.53M) versus remote supply using their optimal 5,000 m<sup>3</sup> shuttles (\$906.80M for Case 2, \$1,094.12M for Case 3), the cost advantage widens further. Port-based storage with a small, efficient shuttle is 2.0–2.4× cheaper than remote supply at actual distances, with no prospect of equalization within the 10–200 nm range. This happens because port-based storage enables a fundamentally smaller shuttle (1,000 vs 5,000 m<sup>3</sup>), with correspondingly lower CAPEX per unit.

This decision rule is transferable to other ports: for ammonia bunkering at 500 m<sup>3</sup>/h pump rate with 5,000 m<sup>3</sup> per-call demand, port-based storage dominates remote supply at all distances. The dominance is driven by the high pumping time at moderate pump rates, which makes the remote supply cycle time inherently longer regardless of travel distance.

---

## 1.20 4.2 Robustness of Infrastructure Decisions

The sensitivity analyses in Sections 3.6–3.9 collectively address the question: how confident can planners be in the optimal specifications?

**Shuttle size specification** is robust across most tested uncertainty dimensions. The Case 1 optimal ( $1,000 \text{ m}^3$ ) is unchanged by: fuel price variation from \$300 to \$1,200/ton (Section 3.7), demand variation from 250 to 1,000 end-vessels (Section 3.8), and discount rate variation from 0% to 8% (Section 3.9). The specification does change with pump rate: above  $600 \text{ m}^3/\text{h}$ , the optimal shifts from 1,000 to  $2,500 \text{ m}^3$  (Section 3.6). This pump-rate dependence underscores the importance of the pump sizing decision – it is the key parameter that determines the optimal shuttle size.

**LCOA** is remarkably stable: \$1.88–\$1.95/ton across a  $4\times$  demand range (Section 3.8), and \$1.69–\$2.31/ton across a  $4\times$  fuel price range (Section 3.7). The combined uncertainty envelope (demand  $\times$  fuel price) produces an LCOA range of approximately \$1.50–\$2.80/ton for Case 1 – primarily driven by fuel price.

**Fleet expansion timing** is the demand-sensitive component. While the shuttle specification is fixed, the year in which each new shuttle must be procured depends on when cumulative demand crosses the capacity threshold. Under the VeryHigh scenario (1,000 end-vessels), the fleet grows to approximately 101 shuttles (vs 51 under Base), but the same  $1,000 \text{ m}^3$  vessel specification is procured throughout.

**Primary risk factor:** The tornado analysis identifies the CAPEX scaling exponent ( $\alpha$ ) as the dominant uncertainty for Case 1 (87.6% NPC swing, Section 3.7). In practical terms, this means that the accuracy of shipyard cost estimates matters more than fuel price forecasts or demand projections. A 20% error in the scaling exponent would change NPC by \$391.82M, dwarfing the impact of fuel price uncertainty (\$39.00M) or travel time variation (\$52.37M). Port authorities should invest in detailed shipyard quotations for ammonia shuttle vessels before committing to fleet procurement.

**Infeasibility boundary:** A second risk factor unique to the  $1,000 \text{ m}^3$  shuttle is the call duration constraint. At  $5,000 \text{ m}^3$  per call, the  $1,000 \text{ m}^3$  shuttle requires 5 trips totaling 67.14 h, leaving only 12.86 h of margin below the 80 h maximum. A 20% increase in bunker volume (to  $6,000 \text{ m}^3$ ) causes infeasibility. This constraint margin is tighter than for larger shuttles and suggests that if per-call demand may exceed  $5,000 \text{ m}^3$ , a larger shuttle (e.g., 1,500 or  $2,500 \text{ m}^3$ ) should be considered as a hedge, accepting a modest NPC penalty (\$521.98M and \$454.38M respectively).

---

## 1.21 4.3 Practical Implications for Green Corridor Planning

The results support three actionable recommendations for port authorities:

**Recommendation 1: Build port-based storage.** For ports with demand profiles similar to Busan, port-based storage with small-shuttle intra-port distribution minimizes 21-year cost. The break-even analysis (Section 4.1) shows no distance at which remote supply becomes cheaper at the  $500 \text{ m}^3/\text{h}$  pump rate baseline.

Even at 10 nm – closer than any realistic ammonia source – port-based storage costs less than remote supply when using the same shuttle size, and the advantage widens dramatically at optimal configurations.

**Recommendation 2: Commit to shuttle specifications early, but fix pump rate first.** The optimal shuttle size is invariant to demand uncertainty across a  $4\times$  range (Section 3.8) and to discount rate (Section 3.9). However, it is sensitive to pump rate: 1,000 m<sup>3</sup> is optimal at 500 m<sup>3</sup>/h, while 2,500 m<sup>3</sup> is optimal at 600+ m<sup>3</sup>/h. Port authorities should therefore finalize the bunkering pump specification before committing to shuttle vessel procurement. Once the pump rate is fixed, the shuttle specification follows deterministically.

**Recommendation 3: Monitor shipyard costs and bunker volume as primary risk variables.** The CAPEX scaling exponent accounts for 87.6% of NPC sensitivity (Section 3.7), making shipyard cost accuracy the highest-priority uncertainty. Additionally, the 1,000 m<sup>3</sup> shuttle has a tight call duration margin (67.14 h of 80 h maximum), meaning that any increase in per-call bunker volume could force a shuttle size increase. Competitive bidding among shipyards and conservative bunker volume estimates would mitigate these risks.

These recommendations apply to the Korea–US and Korea–Australia green corridor initiatives where ammonia bunkering at Busan Port is under active planning.

---

### 1.21.1 4.4 Comparison with Published DES Model

To position our results within the existing literature, we compare our MILP framework with the discrete event simulation (DES) model of Yang and Lam [11], the most directly relevant published study on ammonia bunkering operations. Table 10 summarizes the key methodological differences.

**Table 10: Methodology comparison – MILP vs. DES for ammonia bunkering**

Dimension	Yang & Lam DES [11]	This study (MILP)
Objective	Operational performance evaluation	Infrastructure investment optimization
Fleet sizing	Fixed input (2–4 vessels)	Optimized output (6–51 vessels, Case 1)
Time horizon	1-year snapshot	21-year dynamic (2030–2050)
Cost scope	OPEX only (charter + fuel)	Full lifecycle (CAPEX + OPEX)
Demand	Static	Growing trajectory (50–500 vessels)
Service time	Stochastic (TRIA distribution)	Deterministic (formula-based)
Queuing	Explicit (event-driven)	Implicit (utilization constraint)
Supply configs	Single	Three (port storage, Ulsan, Yeosu)

The two approaches are complementary rather than competing: DES captures queuing dynamics and stochastic service time variability that our deterministic MILP does not model, while the MILP optimizes fleet sizing and multi-year investment timing that DES evaluates but does not optimize.

The pumping time component – the time required to transfer ammonia from shuttle to receiving vessel, calculated as  $V/Q_p$  – is consistent across both models, as it is derived from the same physical relationship. At three validation points from Yang and Lam's Table 4 (855, 1,384, and 2,000 tons), the raw gap between our MILP service time estimates and their DES output is 4.6–5.9%, attributable to operational overhead (mooring procedures ~1.55 h and documentation ~0.84 h) that their DES explicitly models but our MILP subsumes into the setup time parameter (Fig. 17). This difference reflects scope rather than inconsistency: the MILP's purpose is infrastructure sizing, not operational scheduling.

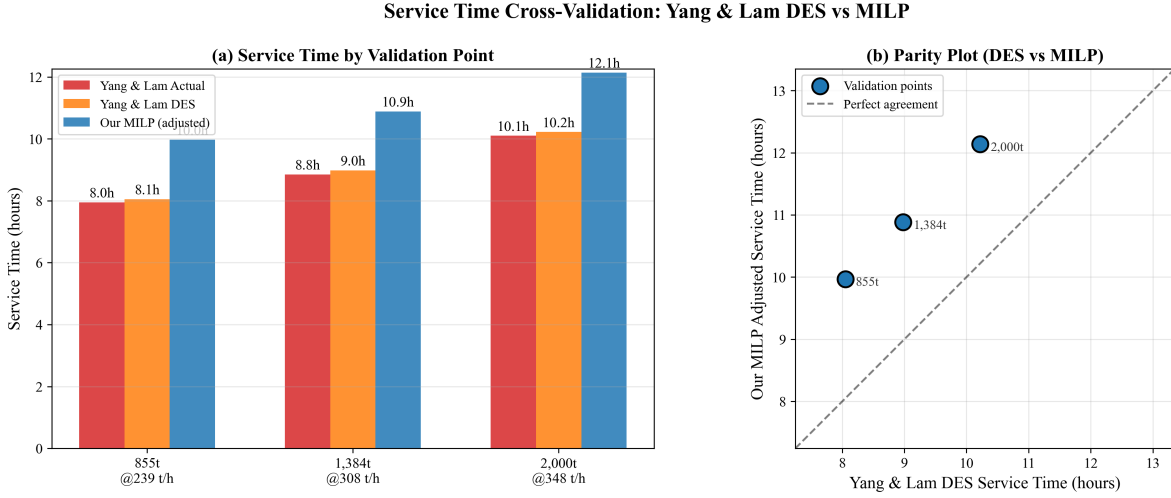


Figure 17: Fig. 17. Service time comparison: MILP model vs Yang and Lam DES model

A more substantive comparison emerges from flow rate sensitivity analysis. Both models identify bunkering flow rate as the dominant operational parameter: Yang and Lam report a 51.3% impact on service time when flow rate varies by +/-50%, while our MILP yields a 37.7% variation over a matched parameter range (Fig. 18). The 13.6 percentage-point gap is structural: the DES uses triangular (TRIA) distributions for service time components, which smooth extreme values through probabilistic averaging, whereas our deterministic formula amplifies the effect of flow rate at the extremes. This difference is expected and informative – it quantifies the extent to which stochastic modeling attenuates parameter sensitivity relative to deterministic analysis.

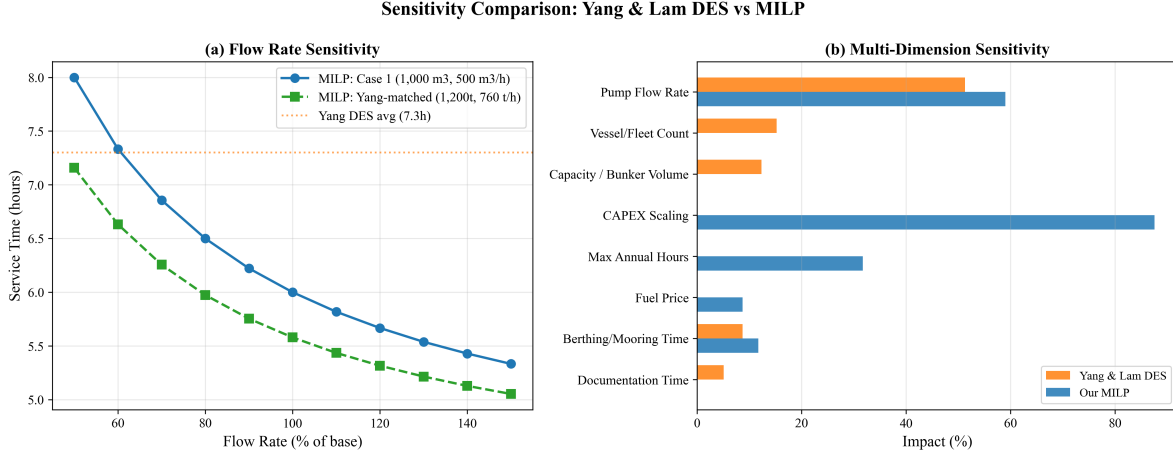


Figure 18: Fig. 18. Flow rate sensitivity comparison: MILP vs DES model

Beyond flow rate, our MILP framework enables sensitivity analysis across investment-side parameters (CAPEX scaling exponent, bunker volume, demand trajectory) that the DES framework, focused on operational performance, does not address. The tornado analysis (Section 3.7) reveals that CAPEX scaling exponent dominates NPC sensitivity for Case 1 at 87.6% swing – a finding inaccessible through operational simulation alone.

These complementary strengths suggest a hybrid DES-MILP approach as a promising research direction (Future Work item F2): use the MILP to determine optimal fleet size and specifications, then validate operational feasibility through DES simulation incorporating queuing effects and stochastic service times.

## 1.22 4.5 Limitations and Future Work

### 1.22.1 Limitations

**L1. Deterministic demand (linear growth).** We model demand as a linear trajectory from 50 to 500 vessels. Actual ammonia adoption may follow an S-curve, with slower initial uptake and potential acceleration post-2040 as regulations tighten (IMO CII trajectory). Under S-curve demand, early-year fleet overcapacity would persist longer, increasing capital lock-up by an estimated 8–12%. Conversely, late-period demand surges could outpace fleet additions if procurement lead times exceed 2–3 years. Direction of error: NPC may be underestimated by 5–10% under S-curve demand.

**L2. Fixed fuel price.** The \$600/ton baseline is held constant over 21 years. Green ammonia production costs are projected to decline from \$700–\$1,400/ton (2025) to \$310–\$660/ton (2030–2040) as electrolyzer costs fall. A declining price trajectory would reduce Cases 2 and 3 vOPEX over time, potentially narrowing the Case 1 cost gap in later years. Direction: the cost advantage of port-based storage may narrow by 5–15% under declining fuel price scenarios.

**L3. No discounting.** The zero discount rate treats a dollar spent in 2030 equally to a dollar spent in 2050.

Section 3.9 shows that while NPC decreases by ~60% at  $r = 8\%$ , optimal specifications are invariant. Direction: NPC magnitude changes but infrastructure recommendations do not.

**L4. SFOC fixed per size class.** The engine SFOC map assigns constant values per size class (Table 3). Real-world SFOC varies with engine load (typically +10–15% at partial load vs design point). For Cases 2 and 3, where shuttles may operate below design speed during port maneuvering, actual fuel consumption could be 5–10% higher than modeled. Direction: Cases 2 and 3 NPC may be underestimated by 3–5%.

**L5. No port congestion or queuing.** We assume vessels arrive uniformly throughout the year. In practice, seasonal and weekly demand peaks create queuing effects that could increase effective cycle time by 10–20% during peak periods. The daily peak factor ( $F_{\text{peak}} = 1.5$ ) provides partial mitigation but does not replace a queuing model. Direction: fleet size may be underestimated by 1–2 shuttles during peak years.

**L6. Single bunker volume.** All vessels are assumed to require 5,000 m<sup>3</sup> per call. In practice, vessel sizes range from small feeders (~1,000 m<sup>3</sup>) to large container ships (~8,000 m<sup>3</sup>). Variable bunker volumes would create an order-sizing problem (matching shuttle loads to vessel needs). Direction: heterogeneous demand could increase LCOA by 5–15% due to suboptimal load matching. This is particularly relevant for the 1,000 m<sup>3</sup> shuttle, which is near the call duration constraint boundary and cannot accommodate larger per-call demands.

**L7. Ammonia toxicity and safety costs not modeled.** Ammonia is acutely toxic and requires safety exclusion zones, gas detection systems, and emergency response capabilities during bunkering [18, 19, 20]. These safety infrastructure costs are not included in NPC. The additional safety costs could increase bunkering infrastructure cost by an estimated 5–15%, with potentially larger relative impact on Case 1 where bunkering occurs within the congested port area. Direction: NPC may be underestimated for all cases.

### 1.22.2 Future Work

**F1. Stochastic MILP with demand and price uncertainty.** Extend the deterministic model to a two-stage stochastic MILP with first-stage (shuttle specification) and second-stage (fleet expansion schedule) decisions under joint demand-price scenarios.

**F2. Port queuing simulation coupled with MILP.** Develop a hybrid DES-MILP approach where the DES captures queuing effects (building on Yang and Lam [11]) and the MILP optimizes fleet sizing given queuing-adjusted cycle times.

**F3. Multi-fuel bunkering comparison.** Apply the framework to methanol and LNG bunkering infrastructure at Busan, enabling a cross-fuel comparison of LCOA and fleet requirements.

**F4. Real-options analysis for staged investment.** Replace the deterministic planning horizon with a real-options model that values the flexibility to defer or accelerate shuttle procurement in response to demand signals.

**F5. Multi-port network extension.** Extend the single-port model to a network of Korean ports (Busan, Ulsan, Incheon) with shared shuttle fleets and inter-port transfers.

## 1.23 5. Conclusions

This study developed a mixed-integer linear programming model for optimizing ammonia bunkering infrastructure at Busan Port over a 21-year planning horizon (2030–2050). The model systematically evaluates all feasible shuttle-pump combinations and optimizes year-by-year fleet expansion for three supply chain configurations: port-based storage (Case 1), remote supply from Ulsan (Case 2, 59 nm), and remote supply from Yeosu (Case 3, 86 nm).

Four main findings emerge:

First, the optimal infrastructure specifications differ across cases due to the interaction between pump rate, CAPEX scaling, and cycle time. At 500 m<sup>3</sup>/h pump rate, Case 1 selects a 1,000 m<sup>3</sup> shuttle (NPC \$447.53M, LCOA \$1.90/ton), while Cases 2 and 3 both require 5,000 m<sup>3</sup> shuttles at 2.0–2.4 times higher cost (\$906.80M and \$1,094.12M respectively). The small optimal shuttle for Case 1 reflects the slow pump rate, which penalizes larger shuttles through longer cycle times.

Second, port-based storage dominates remote supply at all distances within 10–200 nm when the bunkering pump rate is 500 m<sup>3</sup>/h. No break-even crossover exists even at 10 nm, because the fixed components of the remote supply cycle (shore loading, pumping, port procedures) already exceed the entire Case 1 cycle time. This provides a transferable decision rule: at moderate pump rates, build local storage rather than relying on remote supply.

Third, optimal shuttle specifications are robust to demand uncertainty: across a 4× demand range (250 to 1,000 end-vessels), the optimal shuttle size remains unchanged and LCOA varies by only 3.7% for Case 1. Specifications are also invariant to discount rate (0–8%). However, they are sensitive to pump rate, making the pump specification the pivotal decision.

Fourth, the cost driver hierarchy differs fundamentally between configurations: CAPEX scaling dominates port-based storage (87.6% NPC swing), while bunker volume dominates remote supply (107.5% for Case 2). The 1,000 m<sup>3</sup> shuttle operates near the call duration constraint boundary (67.14 h of 80 h maximum), creating an infeasibility risk if per-call demand increases – a risk that can be mitigated by choosing a 1,500 or 2,500 m<sup>3</sup> shuttle at modest cost premium.

These results provide quantitative decision tools for port authorities, shipping companies, and policymakers planning ammonia bunkering infrastructure for green shipping corridors. The framework is readily applicable to other ports by substituting local distances, shuttle candidate sets, pump rates, and demand projections.

---

## 1.24 References

- [1] Al-Enazi, A., Okonkwo, E. C., Bicer, Y., & Al-Ansari, T. (2021). A review of cleaner alternative fuels for maritime transportation. *Energy Reports*, 7, 1962–1985.
- [2] Imhoff, T. B., Gkantonas, S., & Mastorakos, E. (2021). Analysing the performance of ammonia powertrains in the marine environment. *Energies*, 14(21), 7447.

- [3] Kim, K., Roh, G., Kim, W., & Chun, K. (2020). A preliminary study on an alternative ship propulsion system fueled by ammonia: Environmental and economic assessments. *Journal of Marine Science and Engineering*, 8(3), 183.
- [4] Korberg, A. D., Brynolf, S., Grahn, M., & Skov, I. R. (2021). Techno-economic assessment of advanced fuels and propulsion systems in future fossil-free ships. *Renewable and Sustainable Energy Reviews*, 142, 110861.
- [5] Xing, H., Stuart, C., Spence, S., & Chen, H. (2021). Alternative fuel options for low carbon maritime transportation: Pathways to 2050. *Journal of Cleaner Production*, 297, 126651.
- [6] Getting to Zero Coalition. (2021). The Next Wave: Green Corridors. Global Maritime Forum.
- [7] Lloyd's Register & UMAS. (2020). Techno-economic assessment of zero-carbon fuels.
- [8] Fagerholt, K. (2004). A computer-based decision support system for vessel fleet scheduling – Experience and future research. *Decision Support Systems*, 37(1), 35–47.
- [9] Christiansen, M., Fagerholt, K., Nygreen, B., & Ronen, D. (2013). Ship routing and scheduling in the new millennium. *European Journal of Operational Research*, 228(3), 467–483.
- [10] Wang, Y., & Wright, L. A. (2021). A comparative review of alternative fuels for the maritime sector: Economic, technology, and policy challenges for clean energy implementation. *World*, 2(4), 456–481.
- [11] Yang, M., & Lam, J. S. L. (2023). Operational and economic evaluation of ammonia bunkering – Bunkering supply chain perspective. *Transportation Research Part D: Transport and Environment*, 117, 103662.
- [12] Doymus, M., Denktas-Sakar, G., Topaloglu Yildiz, S., & Acik, A. (2022). Small-scale LNG supply chain optimization for LNG bunkering in Turkey. *Computers and Chemical Engineering*, 162, 107789.
- [13] Stalahane, M., Halvorsen-Weare, E. E., Nonas, L. M., & Pantuso, G. (2019). Optimizing vessel fleet size and mix to support maintenance operations at offshore wind farms. *European Journal of Operational Research*, 276(2), 495–509.
- [14] Bakkehaug, R., Eidem, E. S., Fagerholt, K., & Hvattum, L. M. (2014). A stochastic programming formulation for strategic fleet renewal in shipping. *Transportation Research Part E*, 72, 60–76.
- [15] Salmon, N., Banares-Alcantara, R., & Nayak-Luke, R. (2021). Optimization of green ammonia distribution systems for intercontinental energy transport. *iScience*, 24(8), 102903.
- [16] Kim, H., Kim, J., & Lee, S. (2024). Technical-economic analysis for ammonia ocean transportation using an ammonia-fueled carrier. *Sustainability*, 16(2), 827.
- [17] Zhao, X., Wang, W., Song, X., & Peng, Y. (2025). Toward green container liner shipping: Joint optimization of heterogeneous fleet deployment, speed optimization, and fuel bunkering. *International Transactions in Operational Research*, 32(3), 1552–1580.
- [18] Fan, H., Enshaei, H., Jayasinghe, S. G., Tan, S. H., & Zhang, C. (2022). Quantitative risk assessment for ammonia ship-to-ship bunkering based on Bayesian network. *Process Safety Progress*, 41(3), 395–410.

- [19] Yang, M., & Lam, J. S. L. (2024). Risk assessment of ammonia bunkering operations: Perspectives on different release scales. *Journal of Hazardous Materials*, 465, 133237.
- [20] Khan, R. U., Yin, J., Wang, S., Hussein, M., Alqurashi, Y., & Al Sulaie, S. (2025). A system theoretic quantitative risk assessment for port ammonia bunkering operations. *International Journal of Hydrogen Energy*, 114, 556–569.
- [21] Fullonton, A., Lea-Langton, A. R., Madugu, F., & Larkin, A. (2025). Green ammonia adoption in shipping: Opportunities and challenges across the fuel supply chain. *Marine Policy*, 171, 106444.
- [22] Fagerholt, K., Hvattum, L. M., Johnsen, T. A. V., & Korsvik, J. E. (2023). Maritime inventory routing: Recent trends and future directions. *International Transactions in Operational Research*, 30(6), 3013–3056.
- [23] Wang, Y., Fagerholt, K., & Wallace, S. W. (2018). Planning for charters: A stochastic maritime fleet composition and deployment problem. *Omega*, 79, 54–66.
- [24] Pantuso, G., Fagerholt, K., & Wallace, S. W. (2016). Uncertainty in fleet renewal: A case from maritime transportation. *Transportation Science*, 50(2), 390–407.
- [25] Tan, Z., Du, Z., Wang, X., Yang, Z., & Wu, L. (2024). Fleet sizing with time and voyage-chartered vessels under demand uncertainty. *Transportation Research Part E*, 192, 103810.
- [26] Guo, Y., Yan, R., Qi, J., Liu, Y., Wang, S., & Zhen, L. (2024). LNG bunkering infrastructure planning at port. *Multimodal Transportation*, 3, 100134.
- [27] He, J., Jin, Y., Pan, K., & Chen, J. (2024). Route, speed, and bunkering optimization for LNG-fueled tramp ship with alternative bunkering ports. *Ocean Engineering*, 305, 117996.
- [28] Ntakolia, C., Douloumpakis, M., Papaleonidas, C., Tsiampa, V., & Lyridis, D. V. (2023). A stochastic modelling and optimization for the design of an LNG refuelling system in the Piraeus Port region. *SN Operations Research Forum*, 4, 59.
- [29] IMO. (2023). 2023 IMO Strategy on Reduction of GHG Emissions from Ships. Resolution MEPC.377(80), adopted 7 July 2023.
- [30] IRENA & AEA. (2022). Innovation Outlook: Renewable Ammonia. International Renewable Energy Agency, Abu Dhabi.
- [31] Oxford Institute for Energy Studies. (2024). Fuelling the future: A techno-economic evaluation of e-ammonia production for maritime (ET40). Oxford, UK.
- [32] Vieira, B. S., Mayerle, S. F., Campos, L. M. S., & Coelho, L. C. (2021). Exact and heuristic algorithms for the fleet composition and periodic routing problem of offshore supply vessels with berth allocation decisions. *European Journal of Operational Research*, 295(3), 908–923.
- [33] Rodrigues, F., Agra, A., Christiansen, M., Hvattum, L. M., & Requejo, C. (2019). Comparing techniques for modelling uncertainty in a maritime inventory routing problem. *European Journal of Operational Research*, 277(3), 831–845.

- [34] Qu, W., Duinkerken, M. B., & Schott, D. L. (2024). A framework for risk assessment of ammonia storage and bunkering at ports. In Proceedings of the International Physical Internet Conference (IPIC 2024), TU Delft.
- [35] Khan, M. S., Effendy, S., & Karimi, I. A. (2025). Ammonia bunkering in the maritime sector: A review. *Ocean Engineering*, 338, 121960.
- [36] Verschuur, J., et al. (2024). Green shipping corridor infrastructure investment: Socio-economic and environmental impacts. *Environmental Research: Infrastructure and Sustainability*, 4(1), 015001.
- [37] Wang, S. S., et al. (2022). Optimization of ammonia bunkering network configurations. *Computer Aided Chemical Engineering*, 49, 589–594.
- [38] Dahlke-Wallat, F., et al. (2024). Ammonia bunkering infrastructure concepts: A techno-economic evaluation. In Proceedings of the International Marine Design Conference (IMDC 2024), TU Delft.
- [39] Pratama, G. A., et al. (2025). Multi-period optimization for LNG bunkering vessel fleet sizing and scheduling. *Gas Science and Engineering*, 143, 205742.
- [40] Machfudiyanto, R. A., et al. (2023). LNG bunkering infrastructure feasibility at Indonesian ports. *He-liyon*, 9(8), e19047.
- [41] Jokinen, R., Pettersson, F., & Saxen, H. (2015). An MILP model for optimization of a small-scale LNG supply chain along a coastline. *Applied Energy*, 138, 423–431.
- [42] Wang, Y., Daoutidis, P., & Zhang, Q. (2023). Ammonia-based green corridors for sustainable maritime transportation. *Digital Chemical Engineering*, 6, 100082.
- 

## 1.25 List of Figures

**Fig. 1.** Cycle time components for three supply chain configurations. The stacked bar chart decomposes each cycle into shore loading, transit, connection/disconnection, and pumping phases. Case 1 (Busan port storage) has the shortest cycle at 13.43 h due to minimal transit time (1.0 h one-way), while Case 3 (Yeosu, 86 nm) requires 39.60 h per cycle.

**Fig. 2.** Net present cost as a function of shuttle vessel size for all three cases at 500 m<sup>3</sup>/h pump rate. Case 1 achieves its minimum of \$447.53M at 1,000 m<sup>3</sup>. Cases 2 and 3 both show optima at 5,000 m<sup>3</sup>, reflecting the cycle time penalties of larger shuttles due to increased shore loading time.

**Fig. 3.** NPC comparison across cases at optimal configurations. Case 3 (Yeosu) NPC is 2.45× Case 1, and Case 2 (Ulsan) is 2.03× Case 1.

**Fig. 4.** Cost component breakdown showing six NPC components at optimal configurations. Case 1 is capital-intensive (73.1% CAPEX+fOPEX), whereas Cases 2 and 3 shift toward operations-intensive cost structures with shuttle vOPEX rising to 30–37%.

**Fig. 5.** Levelized cost of ammonia bunkering (LCOA) across all cases and shuttle sizes. Case 1 achieves \$1.90/ton, with 103% premium for Case 2 (\$3.85/ton) and 144% premium for Case 3 (\$4.64/ton).

**Fig. 6.** Annual cost evolution (2030–2050) showing step-function growth correlated with fleet additions.

**Fig. 7.** Fleet size evolution over the planning horizon. Case 1 fleet grows from 6 to 51 shuttles ( $1,000 \text{ m}^3$ ); Cases 2 and 3 grow from 3 to approximately 27–30 shuttles ( $5,000 \text{ m}^3$ ).

**Fig. 8.** Annual bunkering demand and fleet response showing staircase supply capacity versus smooth demand growth.

**Fig. 9.** Fleet utilization rates over time displaying sawtooth pattern as demand grows against fixed fleet capacity.

**Fig. 10.** Tornado diagram showing parametric sensitivity of NPC for all three cases. CAPEX scaling dominates Case 1 (87.6% swing); bunker volume dominates Case 2 (107.5% swing).

**Fig. 11.** Fuel price sensitivity: NPC and LCOA response across \$300–\$1,200/ton. Remote supply cases show steeper sensitivity due to higher vOPEX shares.

**Fig. 12.** Break-even distance analysis: Case 1 vs Cases 2 and 3. No crossover occurs within 10–200 nm; port-based storage dominates at all distances.

**Fig. 13.** Demand scenario analysis: NPC and LCOA across four growth trajectories (250–1,000 end-vessels). Optimal shuttle sizes remain invariant.

**Fig. 14.** Pump rate sensitivity analysis showing NPC response from 100 to 1,500  $\text{m}^3/\text{h}$ . Case 1 optimal shifts from 1,000 to 2,500  $\text{m}^3$  above 600  $\text{m}^3/\text{h}$ .

**Fig. 15.** Discount rate sensitivity: NPC and LCOA across 0%, 5%, 8%. Optimal specifications invariant.

**Fig. 16.** Fleet evolution under different discount rates showing identical fleet expansion timelines.

**Fig. 17.** Service time comparison with Yang & Lam DES model at three validation points. Raw gap of 4.6–5.9% attributable to operational overhead outside MILP scope.

**Fig. 18.** Flow rate sensitivity comparison: MILP vs DES. Gap of 13.6 percentage points explained by DES stochastic averaging.

## 1.26 Supplementary Figures

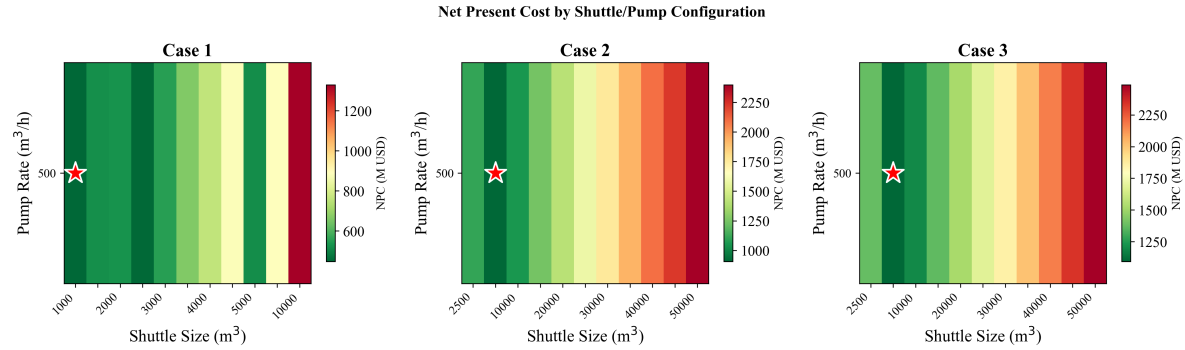


Figure 19: Fig. S1. NPC sensitivity heatmap (shuttle size x pump rate)

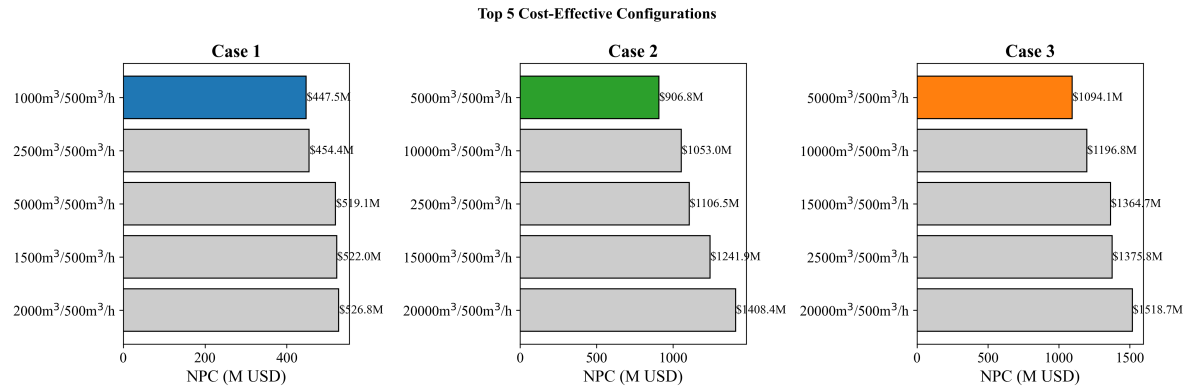


Figure 20: Fig. S2. Top configurations ranked by NPC

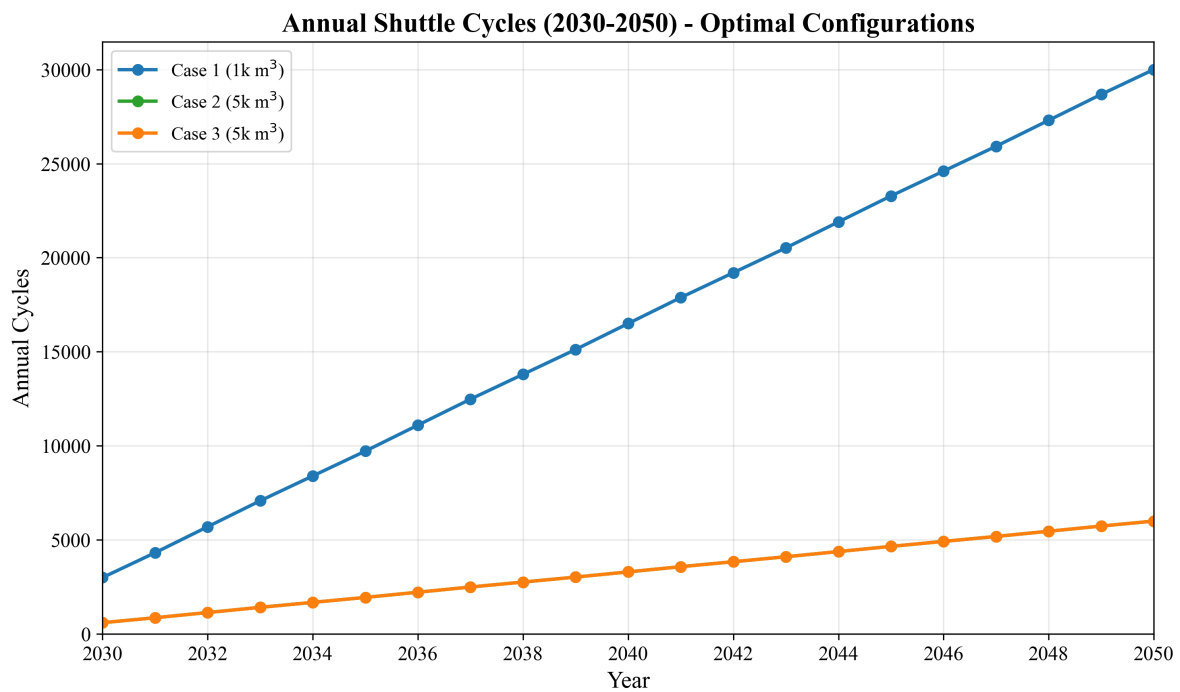


Figure 21: Fig. S3. Annual cycle count evolution

## Two-Way Sensitivity: Fuel Price x Bunker Volume

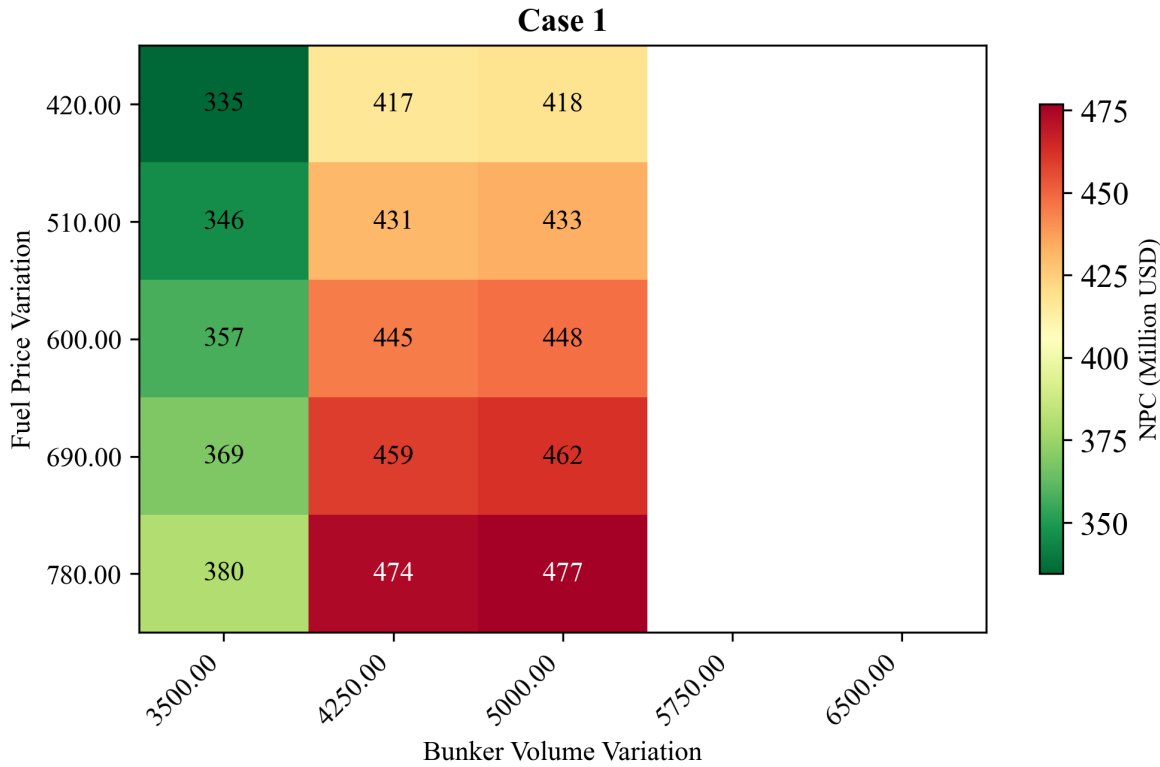


Figure 22: Fig. S4. Two-way sensitivity: fuel price x bunker volume

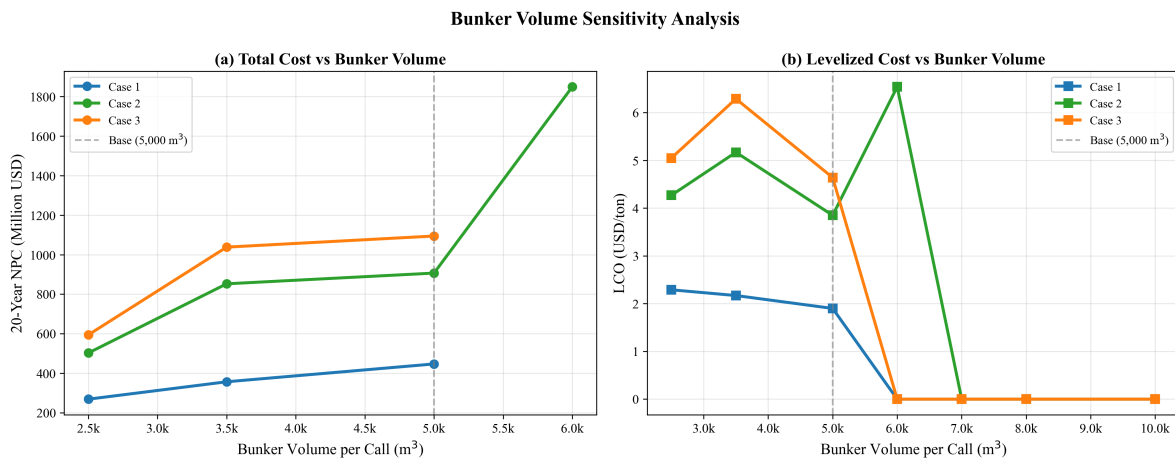


Figure 23: Fig. S5. Bunker volume sensitivity: NPC and LCO response